PHILOSOPHICAL TRANSACTIONS OF THE ROYAL SOCIETY A MATHEMATICAL, PHYSICAL & ENGINEERING SCIENCES

Tides and Waves in The Vicinity of Saint Helena

D. E. Cartwright

Phil. Trans. R. Soc. Lond. A 1971 **270**, 603-646
doi: 10.1098/rsta.1971.0091

TIDES AND WAVES IN THE VICINITY OF SAINT HELENA

By D. E. CARTWRIGHT
National Institute of Oceanography, Wormley, Godalming, Surrey

(*Communicated by Sir George Deacon, F.R.S.—Received* 26 *May* 1971)

(With an appendix by J. S. Driver)

[Plate 13]

CONTENTS

Sea-bed pressures taken close to the shore-line at St Helena over 39 days are analysed for information on tides, swell, and medium frequency waves.

The tidal records are analysed in conjunction with short records taken by others from Ascension, Trindade and Tristan da Cunha Islands. A nine-year series from Simons Bay, South Africa, is also investigated as a possible reference base. It is found to be partially unsuitable on account of a node in the diurnal tides, previously unsuspected, but this itself is relevant to the diurnal cotidal map. A phenomenal monthly tide at Simons Bay, with sidereal rather than anomalistic monthly periodicity, is also noted. Taking a year's record from Ascension Island as tidal reference, new constants are evaluated for all four islands, and

Vol. 270. A. 1210. (Price £1.25; U.S. $3.25) 50 [Published 16 December 1971

these are used to deduce cotidal maps fo the open South Atlantic. Two types of maps are considered, one a linear interpolation of the constants, the other derived from a locally forced tide (modified by the Earth tide) and a pair of Poincaré waves calculated for a 'β-plane' approximation, assuming constant depth. Although not entirely realistic, the latter scheme fits the semi-diurnal tide data very closely, but not the diurnal data. Both types of map confirm positive semi-diurnal amphidromes, according with the computations of Pekeris and Accad and of Bogdanov and Magarik, and negative diurnal amphidromes according with Dietrich's maps.

Tidal records made at St Helena in 1761 by Maskelyne and Mason provide a unique opportunity to search for possible instabilities in the ocean tides. By careful comparison of the two sets of data, it is concluded that the semi-diurnal tides are virtually unchanged, but there is a significant change in phase of about 10° at all diurnal frequencies which may point to an instability in the diurnal modes in the Atlantic, as suggested by Garrett & Munk from other considerations.

A frequency-time plot of the swell wave spectra shows dispersive ridges as found in the Pacific and elsewhere. These point to storm origins principally in the South Pacific and the North Atlantic Oceans. Large-scale 'rollers' were not encountered, but there was some evidence that they have similar origins.

Medium frequency waves (1 to 30 mHz) were recorded simultaneously at two points round the St Helena coast. Their spectra and coherence were studied with a view to identifying trapped modes. A theory is evaluated for waves trapped by a circular island with paraboloidal shelf (as approximately at St Helena) in contrast to the vertical wall models studied by Longuet-Higgins and others. Its main feature is that resonance peaks are much flatter than in the vertical wall cases, and do not increase with frequency. Analysis of the data shows features in common with the theory up to about 3 mHz and at some other energy peaks, but at higher frequencies there is evidence for energy leakage due to topographical roughness.

1. Introduction

Towards the end of 1969, J. S. Driver and the author† took 39 days continuous records of sea-bed pressure off the shoreline of the island of St Helena (15° 58′ S, 5° 43′ W). This paper describes the results of analysing these unique records from a part of the ocean which has been on the whole neglected by marine scientists.

The original motive for the expedition sprang from seeing an early draft of the cotidal map for the M_2 component in the world oceans recently computed by Pekeris & Accad (1969). Their solution of Laplace's tidal equations without recourse to any empirical data differs from the results of all other investigators (e.g. Dietrich 1944; Hansen 1952; Bogdanov & Magarik 1967; Hendershott 1970), which depend on coastal tide data, in showing a positive amphidrome in the tropical South Atlantic. All cotidal maps suffer from lack of comparative records from the open sea, and this feature presents a rare situation where a few suitably placed measurements could be critical. In the foreseeable future one hopes for open-sea data from a network of stations along chosen boundaries (Hansen 1966) from bottom pressure capsules (Eyriès 1968; Snodgrass 1968; Collar & Spencer 1970; Filloux 1971), or possibly from satellite altimeters (Greenwood *et al.* 1969), but for the present one must make the most of the oceanic islands, where the logistics of tide measurement are far easier.

Four small islands span the area of the Pekeris–Accad amphidrome, Ascension (7° 55′ S, 14° 25′ W), Trindade (20° 30′ S, 29° 20′ W), Tristan da Cunha (37° 2′ S, 12° 18′ W), and St Helena. See figure 9 for global maps. All are volcanic, rising steeply out of deep water, and therefore present no serious problems of tidal diffraction. However, only the first two possess reliable constants derived from recent records. M_2 constants for the second two islands (quoted by Pekeris & Accad) are given in the 1938 edition of the *Admiralty tide tables*, part 2, with the designation 'inferred' but were omitted from subsequent editions as unreliable. The tidal ranges are small and there is no local demand for accurate predictions. Further inquiries revealed a 15-day record of hourly sea levels taken at Tristan Island in March 1968 by the U.S. Coast and

† K. Tipping of N.I.O. also assisted in the early stages.

Geodetic Survey during a satellite triangulation exercise. This series, though minimally short for analysis, is just adequate for the present purpose. The only existing records from St Helena are the tide-pole observations made by Maskelyne and Mason (Maskelyne 1762*b*) during their voyages relating to the Venus transit of 1761. The situation demanded new measurements, and so our recording expedition was planned. Transport to the island was kindly provided by the Hydrographer of the Navy in H.M.S. *Vidal*, which was making a voyage round the Cape. The Navy also provided some useful supporting measurements.

Since we used pressure sensors for tidal measurement, we also took the opportunity to record the high frequency (0.03 to 0.20 Hz) pressure variations due to swell. The swell waves, or 'rollers', of the South Atlantic are well known to mariners, but they have inspired little scientific study, and in fact their origin is quite unknown to the inhabitants of St Helena, where the Jamestown waterfront is frequently damaged and boats often capsized by rollers. The Admiralty's *Africa Pilot*, vol. 2, 1963 edition, states (p. 37) that they 'break with great violence on (the islands') lee sides, and arrive without any apparent warning'. 'Their origin has been the subject of much discussion, and the general conclusion arrived at is that these huge ocean ripples are the progressive undulations caused by distant storms, in the Atlantic oceans of either hemisphere.' We have not seen any printed account of such discussion, but our main object in recording the swell waves was to substantiate the stated conclusion by scientific analysis.

We also recorded the pressure variations in an intermediate† spectral band, roughly 10^{-4} to 10^{-2} Hz, for an investigation of 'island-trapped' waves. These fall into the wide and growing class of possible oceanic motions which have been profoundly studied in theory but scarcely observed in nature. The theory is especially well developed for a steep-sided circular island surrounded by extensive water of uniform depth (Longuet-Higgins 1967; Summerfield‡ 1969). St Helena approaches these conditions better than most real islands, in fact considerably better than Macquarie Island (54° S, 159° E), where a 6 min oscillation has inspired much of the theoretical work. We hoped therefore to obtain natural measurements against which the theory can be reasonably tested.

The main outline of the paper is as follows. After an account of the instruments and their deployment, the discussion is divided into three main sections, dealing with tides, swell and trapped waves, in that order. The tidal section comprises an account of the interconnected analysis of data from all four islands mentioned earlier and also from Simons Bay, South Africa, using new techniques; a comparison of the results with those of a new analysis of Maskelyne's historic data; and finally the fitting of local cotidal maps to the island data alone, and their comparisons with maps by other authors. The analysis of swell consists mainly in the construction of a spectral energy-time diagram in the manner of Munk, Miller, Snodgrass & Barber (1963), and its interpretation in terms of storm distances. The section devoted to trapped waves first describes computations of the resonances one might expect for the nearly paraboloidal shape of St Helena's offshore topography, then discusses what features of the measured medium-wave spectra support them.

† Such ocean waves used to be termed 'long' (Munk 1962) or 'low-frequency' in the literature of 1955–65, but the later attention given to frequencies below 10^{-5} Hz (1 c/d) now makes both terms ambiguous.

‡ Summerfield also studies the elliptical island.

PHILOSOPHICAL TRANSACTIONS OF THE ROYAL SOCIETY A MATHEMATICAL, PHYSICAL & ENGINEERING SCIENCES

2. Recording logistics

(*a*) *Instrumentation*

St Helena has no harbour to protect a conventional stillwell tide-gauge, so we used a frequency-modulated capacitance plate pressure transducer of N.I.O. design (Harris & Tucker 1963), fixed to a heavy tripod which was lowered to the bottom at a depth of 9 m, about 100 m offshore. This was connected by cable to Jamestown wharf, where the island government allowed us to house a recorder unit in the 'Landing Waiter's Office'. Both tide and swell variations were taken from the same pressure signal by means of low- and high-pass filters, with cutoff frequencies at about 0.02 Hz, and fed to pen recorders with appropriate chart speeds. The electrical processing and recording unit, which included a crystal-controlled clock, is described in appendix A by J. S. Driver, who designed it.

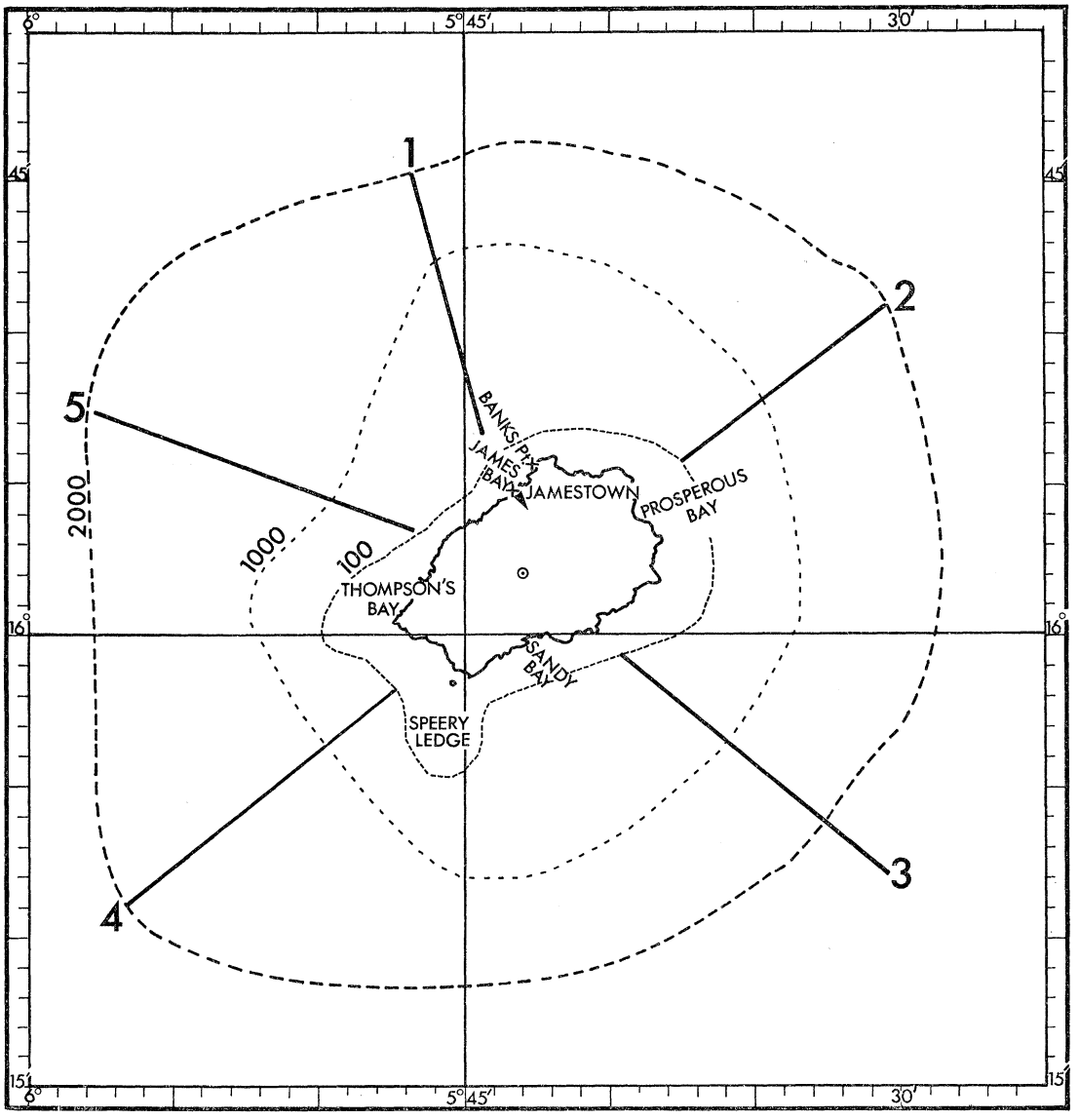

Figure 1. Left. For legend see opposite.

PHILOSOPHICAL TRANSACTIONS OF THE ROYAL SOCIETY A MATHEMATICAL, PHYSICAL & ENGINEERING SCIENCES

An important auxilliary piece of tide recording equipment was a portable stillwell, consisting of a long rigid polypropylene tube of 80 mm internal diameter, closed at the bottom but for a 4 mm hole, and held vertical by a light rigid framework at the top which could be rested securely on one of the wharf steps. The time constant of the well was about a minute, and the water level inside was measured relative to the step level by a flexible tape with electrical contact indicator. This device was read hourly over about half a tidal cycle every day, as a direct reference to land datums and as a measure of 'drift' in the pressure sensor. Land datums, in the form of freshly cut bench marks with levelling figures, were provided by naval staff from H.M.S. *Vidal*.

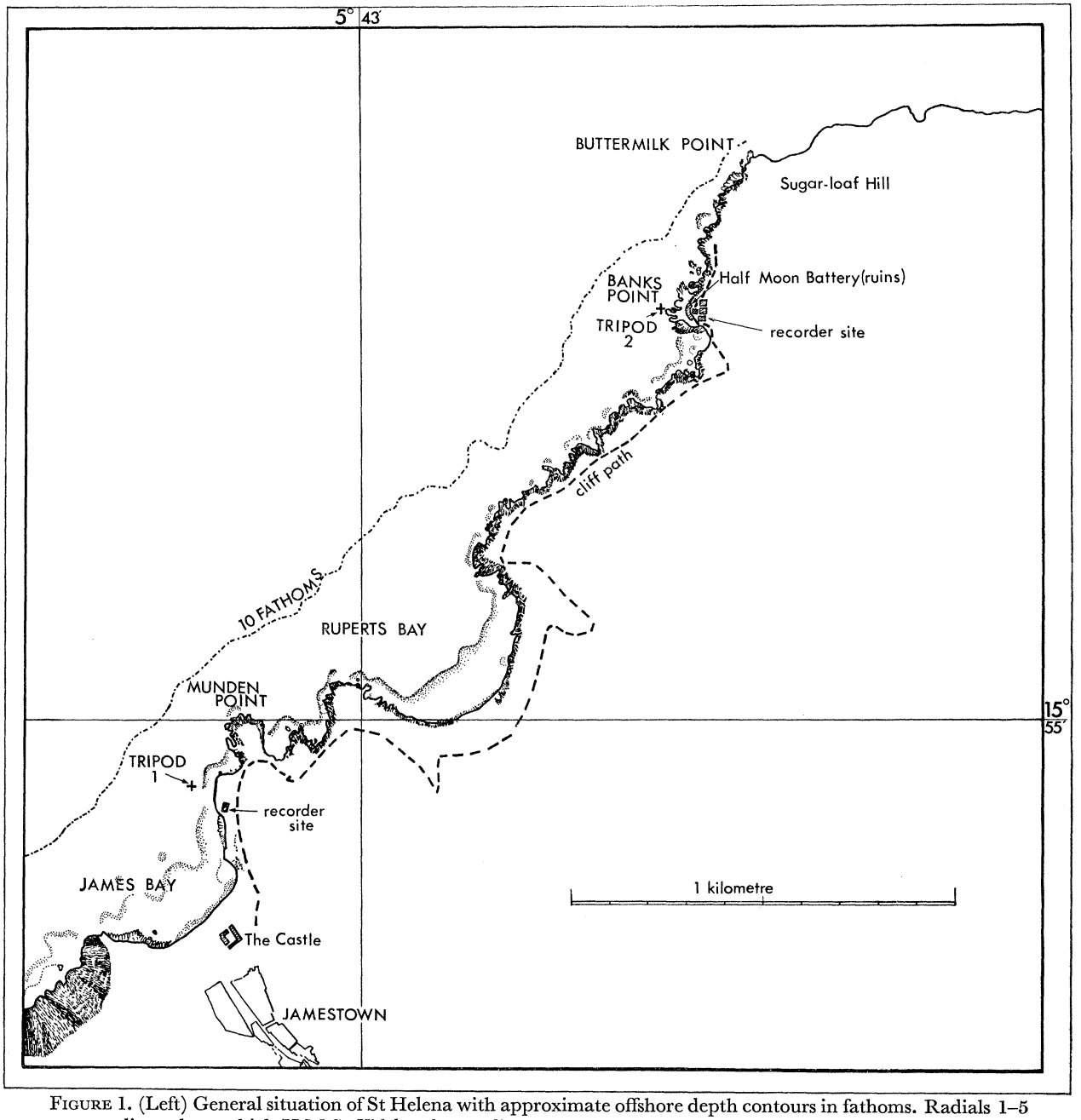

FIGURE 1. (Left) General situation of St Helena with approximate offshore depth contours in fathoms. Radials 1–5 are lines along which H.M.S. *Vidal* took soundings 3 November 1969. (Right) Positions of tripods 1 and 2, bearing pressure recorders.

For the medium wave measurements it was desirable to have two recorders working simultaneously a few kilometres apart round the coast, in order to distinguish between true trapped waves and local oscillations produced by the nonlinear effects of swell, which are strong close to the shore. It was not convenient to duplicate the electrical recorder, and so we took two further pressure recorders of a much simpler kind, each consisting of a limp rubber tyre held near the sea bed and connected by airline to an aneroid pen recorder on shore. Oil-filled capillary tubes of identical time constants (about 30 s) damped out the higher frequency wave motions. These recorders, of standard N.I.O. design, are insensitive to temperature changes and are entirely mechanical in operation; useful assets in the remote and exposed location necessary for at least one of them.

One tyre was attached to the same tripod (1) in James Bay (see maps, figure 1) and used the same recording site as the electrical instrument, but the island's rugged coastline gave us difficulty in finding a convenient site for tripod (2). Rupert's Bay has the only beach-strip reached by road, but this is too close to the James Bay site. Sandy Bay can be reached on foot but is continually pounded by breaking waves from the southeast Trade Winds, which prevented us laying a tripod there. Thompson's and Prosperous Bays are protected from the trade wind seas, but were found to be too hard of access by land for the necessary daily visits to the recorder. Banks Point was finally chosen as a compromise between accessibility and distance (2 km) from James Bay. The tripod was lowered from a boat to 10 m depth just off the point and the recorder was lodged in the partial shelter of the ruins of Half Moon Battery on the cliff edge, 75 m above sea level.

The pneumatic recorders also registered the tidal variations, providing a third check. They record a differential pressure, which corresponds more strictly to the stillwell measurements than to the electrical records, which are of absolute pressure. However, continuous barograph records confirmed that the two types of pressures differed from a constant only by slow variations of a few centimetres of water and by the 12 h atmospheric tide of about 10 mm amplitude.

(*b*) *Timing and digitization*

The crystal clock was checked daily against radio time signals from Ascension and found to be accurate to a few seconds throughout. We marked the tide records several times each day from this clock. By combination with the stillwell recordings, pneumatic, and barograph records, we derived a continuous series of sea levels at 30 min intervals from 3.5 November to 12.5 December G.M.T.

The swell recorder was switched by programme-clock to run for 160 min twice daily, at about 09h40 to 12h20 and 21h40 to 00h20 G.M.T., from 3.0 November to 9.0 December inclusive. Only two records and some following 9 December had to be rejected on account of electrical faults. The analogue charts were digitized on punched cards at 2.5 s intervals by the 'C.I. Data Centre' of Aldershot.

The pneumatic recorder at James Bay functioned throughout the period as a tide gauge (bar a few hours' faulting), but we did not obtain simultaneous pairs of medium-wave records until 18 November, when the second instrument was installed at Banks Point. These were taken daily from 18 November to 11 December by switching to a fast chart speed from precisely 09h40 to 12h20, and using a carefully synchronized watch carried by walking to Banks Point. Those records selected for their potential interest (see § 5) were digitized 'by eye' at 5 s intervals.

All digital series were checked for smoothness by computer before being subjected to further analysis.

3. Tides

(a) *Reference stations—Simons Bay (South Africa)*

It is desirable to express the tide as a *response* to the gravitational tide potential (Munk & Cartwright 1966), even if ultimately we require only the traditional harmonic constants. To derive the response accurately from a record of only about a month's duration we have to choose a 'reference station', reasonably close in space, at which a long tidal record is available (Cartwright, Munk & Zetler 1969). The assumption here is that the response of the 'reference tide' to the potential can be evaluated with precision and with all refinements such as 3rd degree harmonics and radiational effects, and that the relation of the given station to the reference tide is a fairly simple one, expressible in terms of say two arbitrary constants for each tidal species. These constants can then be derived with fair accuracy by correlating the short record with a noise-free synthesis (prediction) of the reference tide, and the total response of the given tide to the potential is obtained by multiplying the two sorts of response function (admittances). The conversion to 'harmonic' constants H and G follows straightforwardly.

The only long records available for some thousands of miles are from South Africa, where Mr A. M. Shipley of Cape Town University and Mr T. E. Donkin of the South African Navy are building up some local tidal series of good quality on punched cards. I investigated the longest, from Simons Bay (34° 11′ S, 18° 26′ E), which started in 1958. Although Simons Bay turned out to be unsuitable as a reference station for the St Helena area, the results of analysis are not irrelevant to the general problem, and are so interesting as to be worth describing *per se*.

The shape of the admittance function being unknown, and shallow water effects negligible, I evaluated the admittance piecemeal at each tidal 'group' (cycle per month separation). The procedure was similar to that applied to Honolulu by Munk & Cartwright, except that they used the finer resolution into tidal 'constituents' (cycle per year separation). The given hourly sea level data $\zeta(t)$ were transformed to heterodyned complex series for each tidal group (j_1, j_2) by means of the filters (cf. Cartwright & Tayler 1971, equation (15)):

$$H_{j_1,j_2}(t) = \exp\{2\pi\mathrm{i}(j_1 f_1 + j_2 f_2 - j_2 f_3)\, t\}\, 2N^{-1} \sum_{h=-\frac{1}{2}N}^{\frac{1}{2}N} \zeta(t+h)\,(1+\cos\pi h/N)\exp(2\pi\mathrm{i}ph/N), \quad (1)$$

where f_1, f_2, f_3 are a cycle per lunar day, month, and year respectively,

$$N = 1416\,\mathrm{h}\ (59\ \mathrm{d}),$$

$$p = 57j_1 + 2j_2,$$

and

$$j_1 = 1,\ 2 \text{ with } j_2 = -4(1)\,4.$$

The group (j_1, j_2) appears in $H_{j_1,j_2}(t)$ with frequencies reduced by $j_1 f_1 + j_2 f_2 - j_2 f_3$, that is with variations between $\pm 4f_3$, and amplitudes only slightly attenuated by the filter characteristics. Other groups are greatly attenuated, and removed from 'aliasing' by taking t in steps of 5 d.

Corresponding series $G_{j_1,j_2}(t)$ were also computed with $\zeta(t)$ effectively replaced by the spherical harmonic coefficients $c_2^{j_1}(t)$ of the tide generating potential. These were simply computed by use of the new time-harmonic expansions recently computed by Cartwright & Tayler (1971) and the filter characteristic, which for frequency f is

$$F_{j_1,j_2}(f) = \frac{\sin^2\nu\cos\nu\delta}{\sin(\nu+\nu\delta)\sin(\nu-\nu\delta)}\,\frac{S(\pi\delta)}{S(\nu\delta)}, \quad (2)$$

where $\nu = \pi/N$, $S(x) = \sin x/x$, and $\delta = 59f - p$.

The admittances $Z(f)$, assumed constant within each group, were estimated from

$$Z = X + \mathrm{i}Y \sim \langle HG^* \rangle / \langle GG^* \rangle,$$

where the ensemble averages $\langle\ \rangle$ were taken over a 9-year span of t. We also have for each group the quantities

$$\gamma^2 = |\langle HG^* \rangle|^2 / \langle HH^* \rangle \langle GG^* \rangle,$$

$$E_0 = \tfrac{1}{2} \langle HH^* \rangle, \quad E_1 = \gamma^2 E_0, \quad E_2 = (1 - \gamma^2)\, E_0,$$

denoting estimates of 'coherence', 'total energy' (variance), 'coherent energy', and 'non-coherent energy' (or noise), respectively. All these quantities are represented in figure 2 after the manner of Munk & Cartwright (1966).

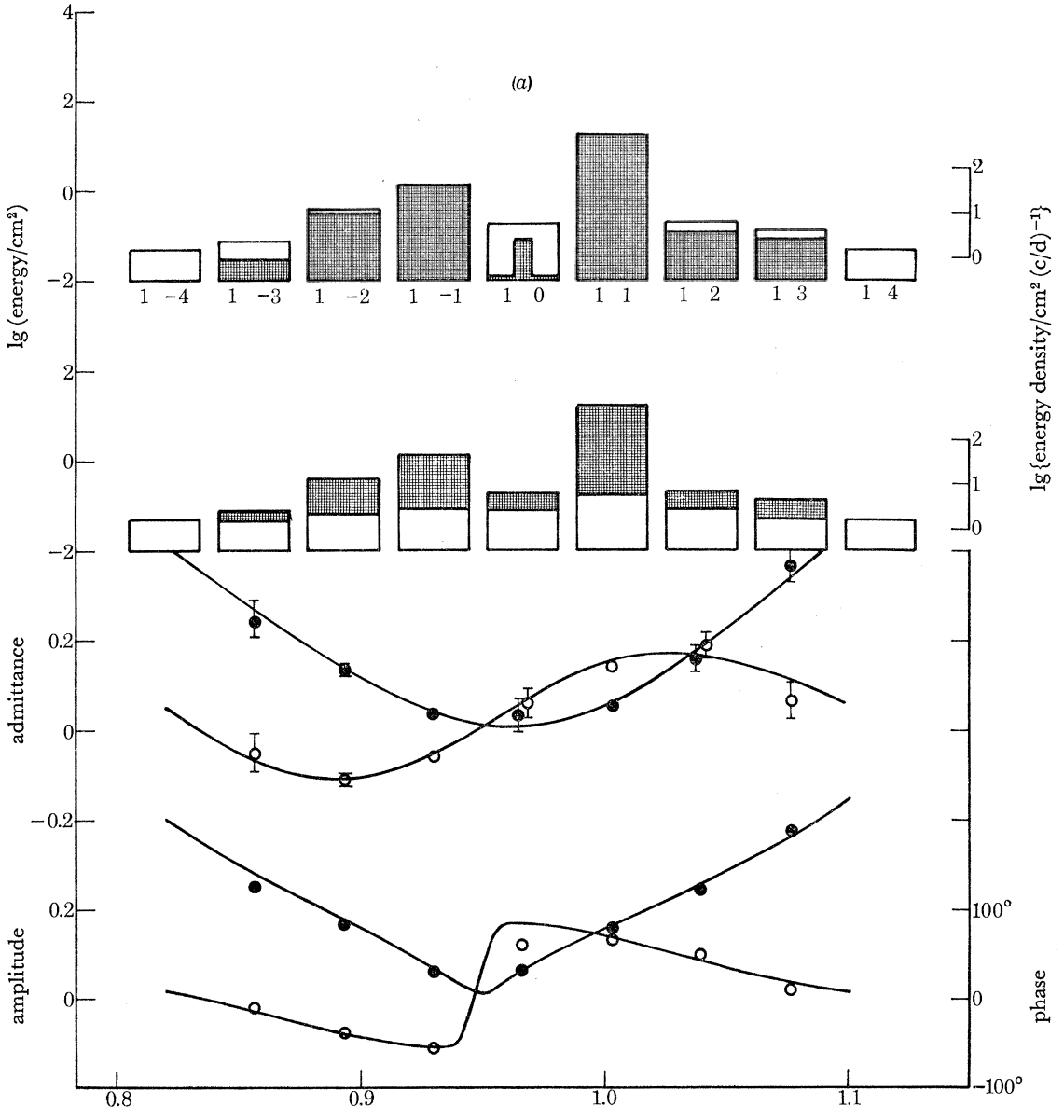

FIGURE 2 (*a*). For legend see opposite.

From the top panel of these figures we see that all groups contain a good share of coherent energy, except for the tidally weak groups $j_2 = \pm 4$ where there is practically none. In the second panels, therefore, the non-coherent energy at the end groups give a good measure of the background noise level, while those in the central groups exhibit the oceanic 'cusp' surrounding the stronger tidal constituents in groups (1 1), (2 0) and (2 2). The lower half of each figure shows the real and imaginary admittances X and Y (with 95 % confidence limits $\propto \gamma^{-2}$), and amplitude $|Z|$ and phase lead arg (Z). The curves here are the results of parallel computations, in which $\zeta(t)$

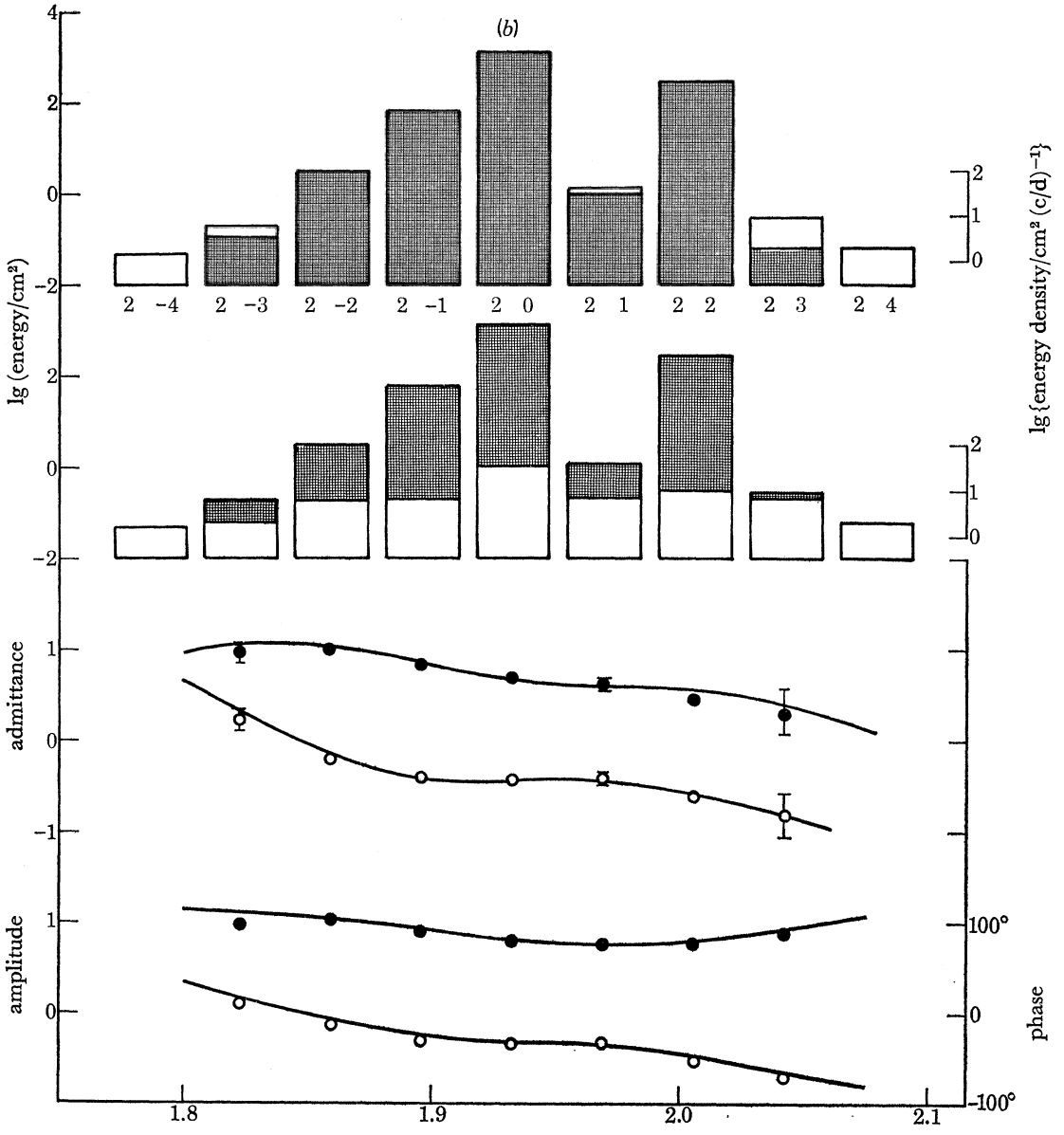

FIGURE 2 (*a*). Energy budget in diurnal tidal groups for Simons Bay, 1959–67. In the top panel, total heights of columns represent total sea level energy E_0, the shaded portions the energy coherent with the gravitational potential $\gamma^2 E_0$. (For groups (1 0) the higher level is coherent with the 3rd degree potential.) In the second panel, the total heights again represent E_0, the unshaded portions incoherent or noise energy $(1-\gamma^2)\,E_0$. The upper pair of curves and circles show the real (black) and imaginary (open) parts of the admittance Z, with 95 % confidence limits for the discrete estimates. The lower pair show amplitude $R = |Z|$ (black) and phase *lead* $\phi = \arg(Z)$ (open). (*b*) as (*a*) for semidiurnal tidal groups.

is correlated directly with time-lagged potential series $c_2^1(t-\tau)$, that is by the 'response method'. They agree well with the individual group values, allowing for the confidence limits, except at the solar groups (1 1) and (2 2), which show the effects of including solar radiational terms in the response analysis. The corresponding constants are listed in appendix C.

The most interesting point in all this is the almost perfect amphidrome at 0.95 c/d, shown by the marked dip in amplitude, the sudden phase change approaching 180°, and the small coherence in the group (1 0). The coherence is so small that I tested this group for coherence with the 3rd degree potential c_3^1, and found it quite significant ($\gamma^2 = 0.49$), as shown by the small black peak in the top panel of figure 2*a*, a rare situation.† Tidal stations situated on amphidromes are few, and this one has apparently not been noticed before because it is tuned sharply enough for the constituents O_1 and K_1 to maintain fair amplitudes, while M_1 is always small and usually contaminated by noise. The sudden change in phase is not remarkable in itself, because it occurs, for example, in the diurnal tides throughout the British Isles (Cartwright 1968) unassociated with any amphidrome.

Little is known about the variation of cotidal maps with continuously varying frequency, but it is reasonable to suppose that the amphidromes traverse a locus in space. One would therefore expect an amphidrome at O_1 or K_1 or both to occur in the ocean not far from Simons Bay. Dietrich (1944) shows neither, but Tiron, Sergeev & Michurin (1967) show an O_1 amphidrome about 15° west of Cape Town which apparently swings round to 15° southeast at K_1. Their study of spatial variations at fixed frequencies therefore possibly accords with the above independent study of frequency variations at a fixed location in space. However, the cotidal maps deduced from the four island stations (§ 3 (*e*) of the present paper) suggest that the K_1 amphidrome is also west of Cape Town.

An admittance curve containing a zero unfortunately makes Simons Bay unsuitable as a reference for our island stations, which are too far removed for such a zero to persist. The admittance for species 2 tides is quite satisfactory and in fact similar to that at St Helena, but there are other places which would serve equally well for semi-diurnal tides. Three years of data from Port Nolloth, some 550 km north of Cape Town, were also analysed, but showed a diurnal admittance very similar to that at Simons Bay.

(*b*) *A monthly tidal phenomenon*

Before leaving Simons Bay, I should like to describe a still more curious feature of its tides. I also applied the procedure described in (*a*) to the cases $j_1 = 0, j_2 = 0, 1, 2, 3$, covering the low-frequency tides, species 0. The immediate result was that coherences with the c_2^0 potential were negligibly small ($< 10^{-2}$) over the 9-year span. This is itself unusual for the quite moderate noise level at the port (about 400 cm² (c/d)$^{-1}$ at group (0 1)), and shows virtually complete suppression of the zonal gravitational tide. The suppression is probably due to the nearness of the zero latitude 35° 16′ of the P_2^0 harmonic, but since the work of Wunsch (1967) one no longer expects monthly and fortnightly tides to adhere very closely to equilibrium values.

In order to check this matter further, I then computed Fourier transforms of the $H_{0,j_2}(t)$ series at $c/9$-year resolution. The harmonic amplitudes for positive frequencies are shown in table 1. Here, harmonic number 0 corresponds to the tidal *constituent* $(0\ j_2 - j_2)$, and increments of 9 give a frequency increment of 1 c/year (0 0 1). The only interest in group (0 0), which is not shown,

† This raises an esoteric point in harmonic prediction. The strongest M_1 line at Simons Bay is not (1 0 0 1 0 0) as at most places, but precisely (1 0 0 0 0 0), amplitude 4 mm.

is the radiational (*Sa*) line of amplitude 28 mm. The absence of any positive anomaly at harmonics 0 and 18 in group (0 2) confirm the insignificance of nonlinear interaction (*MSf*) and linear second degree tide (*Mf*) or (0 2 0 0)† respectively. The surprising anomaly is the 12 mm amplitude at harmonic 9 of group (0 1). This is a monthly tide, but its 'month' is sidereal (0 1 0 0), not anomalistic, (0 1 0 −1).†

The common monthly tide *Mm* is simply due to the elliptically varying distance of the Moon. Since perigee progresses through the stars once in 8.85 years, it loses one cycle in that period, and would appear at harmonic number 8. *Mm* is thus manifestly absent, as expected from the absence of *Mf*, and the sidereal monthly tide observed can only be attributable to the P_3^9 harmonic, which has its strongest line at that frequency. It is very doubtful whether this tide has ever been isolated from tide gauge data before, because its 'equilibrium' amplitude is typically less than 1 mm. The result in question suggests considerable magnification, with the phase lag $G = 290°$ on the Moon's mean longitude. It will be interesting to see if it recurs in the next 9 years of records from Simons Bay, ending 1976, or from elsewhere. Elucidation will have to await a global numerical model for the low-frequency tides.

TABLE 1. NINE-YEAR FOURIER TRANSFORMS (mm) OF $H_{01}(t)$ AND $H_{02}(t)$

harmonic	argument	amplitude	argument	amplitude
0	0 1 −1 0	3.6	0 2 −2 0	3.8
1	0 1 −1 1	2.3	0 2 −2 1	4.6
2	—	5.0	—	2.3
3	—	4.1	—	2.6
4	—	0.5	—	3.8
5	—	5.8	—	5.9
6	—	6.0	—	1.9
7	—	5.0	—	4.7
8	0 1 0 −1	2.0	0 2 −1 −1	4.6
9	0 1 0 0	11.9	0 2 −1 0	3.1
10	0 1 0 0	3.9	0 2 −1 1	4.2
11	—	4.0	—	5.2
12	—	5.0	—	4.4
13	—	4.1	—	4.2
14	—	6.5	—	1.9
15	—	4.0	—	1.9
16	—	3.6	—	3.3
17	0 1 1 −1	4.1	0 2 0 −1	3.3
18	0 1 1 0	3.3	0 2 0 0	4.5
19	0 1 1 1	4.0	0 2 0 1	0.6
20	—	3.9	—	3.9

(*c*) *Ascension Island as a reference station*

A preliminary harmonic analysis of the St Helena tidal data suggested that its admittances are closely related to those of Ascension Island, as judged by Ascension's harmonic constants listed in I.H.B. sheet 2257.‡ Tidal data for Ascension, recorded by the U.S. Coast and Geodetic Survey, consist of 29 days of hourly sea levels, beginning 1.0 February 1959, and a year of all high water and low water times and heights (HLTH) between 21.5 June 1958 and 21.5 June 1959. A year's data from a meteorologically quiet station makes a barely adequate basis for

† Here and in table 1, the four argument numbers refer to f_1, f_2, f_3 and the perigee frequency f_4.

‡ I.H.B. 2257 gives H for M_2 at Ascension correctly in feet but incorrectly in centimetres (see table 2). Pekeris & Accad (1969) quote the incorrect value.

PHILOSOPHICAL TRANSACTIONS OF THE ROYAL SOCIETY A MATHEMATICAL, PHYSICAL & ENGINEERING SCIENCES

independent tidal analysis, so this island, being centrally placed, was finally chosen as reference station for the other three islands considered. The main technical problem was the unfamiliar one of how to extract tidal admittances from a HLTH series.

Two methods were investigated and compared. In the first, a series of Chebychev polynomials to 7th order, $p_7(t)$, was determined for every set of four consecutive extrema $\zeta(t_n)$ such that $p_7(t_n) = \zeta(t_n)$ and $\dot{p}_7(t_n) = 0$ for $n = 1, 2, 3, 4$. $p_7(t)$ was used to interpolate all G.M.T. hourly values occurring between t_2 and t_3, and with 1409 iterations produced a continuous hourly series covering 364 complete days. I then analysed the hourly series by a conventional 'response' method.

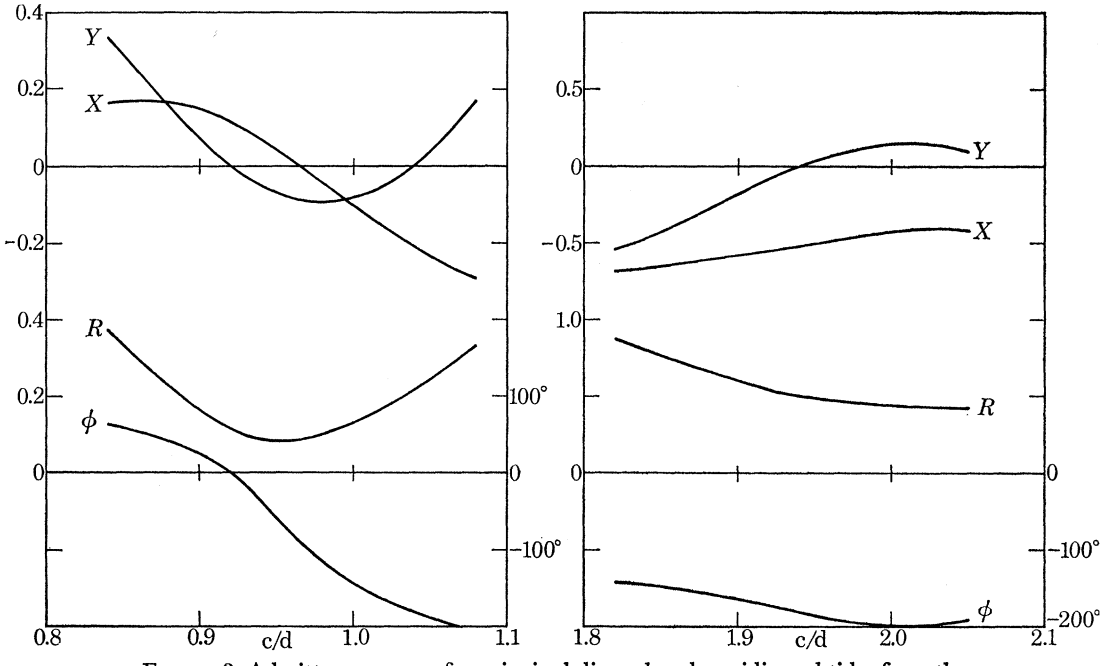

FIGURE 3. Admittance curves for principal diurnal and semidiurnal tides from the one year's record at Ascension Island.

The second method of analysing the HLTH series consisted in minimizing the expression

$$V = \sum_n [\{w_0 + \sum_s w_s c_s^*(t_n) - \zeta(t_n)\}^2 + K^2\{\sum_s w_s \dot{c}_s^*(t_n)\}^2], \tag{3}$$

with respect to the complex 'response weights' w_s, where the $c_s(t)$ represent the set of time-lagged gravitational and radiational potentials used, K is a time constant derived from the residual noise spectrum of the 29-day hourly series, and the outer summation is over all extremum times t_n. (The real part of complex products is understood.) Clearly, this uses the given properties of the data in an optimum way without any assumptions about interpolation, and the only complication is the necessity to compute potentials and their derivatives at arbitrary fractions of an hour. The algebra involved is set out in appendix B.

The response weights w_s resulting from the two methods are similar though of course not identical. I compared their accuracies by spectral analysis of the residual series,

$$\zeta_r(t) = \zeta(t) - \sum_s w_s c_s^*(t)$$

over the recorded 29 days of hourly $\zeta(t)$. The variances of $\zeta_r(t)$ over species 1 were nearly equal,

but the second method gave 19 mm² less than the first in species 2, and therefore 'won' by a small margin. Its weights were adopted for the reference tide, and are listed in appendix C. The principal gravitational admittances are drawn in figure 3. We see that the diurnal amplitude R has a dip near the frequency of the Simons Bay zero, but it is less pronounced, while the phase behaves quite differently and more smoothly. The admittance for species 2 varies smoothly, as at all places in the area.

TABLE 2

Station: James Bay, St Helena Island. 39 days, 3.5 November to 12.5 December 1969.
Reference: tide synthesis for Ascension Island (appendix C).

admittances (station/reference). intervals 1 c/m* (0.0366011 c/d)					principal harmonic constituents				
						station		reference	
c/d	real	imag.	R	$\phi°$	c/d	H/mm	$G°$	H/mm	$G°$
0.8929346	0.7294	0.1724	0.7495	13.30	(Q_1) 0.8932441	7	131.36	9	144.57
0.9295357	0.7434	0.0423	0.7446	3.25	O_1 0.9295357	19	192.77	26	196.02
0.9661368	0.6983	−0.0806	0.7029	353.42					
					(P_1) 0.9972621	10	332.59	15	318.11
1.0027379	0.6032	−0.1706	0.6269	344.21	K_1 1.0027379	31	341.20	50	325.41
1.0393390	0.4781	−0.2091	0.5219	336.38					
recorded variance 1109 mm²									
residual variance 59 mm²									
1.8590714	−0.1709	0.9693	0.9843	100.00					
1.8956725	−0.1317	0.9786	0.9874	97.67	(N_2) 1.8959820	73	63.88	74	161.53
1.9322736	−0.0926	0.9695	0.9739	95.45	M_2 1.9322736	320	81.37	328	176.82
1.9688747	−0.0615	0.9439	0.9459	93.73					
					(S_2) 2.0000000	112	103.09	122	196.00
2.0054758	−0.0450	0.9072	0.9084	92.84	K_2 2.0054758	32	105.54	35	198.38
recorded variance 56 953 mm²									
residual variance 130 mm²									

* c/m = cycle per month; c/d = cycle per day.

Tables 2 to 4 give all the essential details of admittances relative to Ascension and resulting major harmonic constants, in the standard form adopted by Cartwright *et al.* (1969) and by Munk, Snodgrass & Wimbush (1970). The data for St Helena and Tristan da Cunha have already been referred to. Data from Ilha da Trindade were obtained from the Brazilian 'Ministerio da Marinha'. All admittances were obtained by first computing complex tidal syntheses for Ascension,†

$$\xi_m(t), \quad m = 1, 2, 3 = \text{'species'},$$

simultaneous with the given data $\zeta'(t)$, then estimating relative weights w' by least squares to express the tide at that place in the form

$$\xi'(t) = w_0 + \mathrm{Re}\,[w_{10}\xi_1^*(t) + w_{11}\xi_1^*(t-\tau) + w_{20}\xi_2^*(t) + w_{21}\xi_2^*(t-\tau) + w_{30}\xi_3^*(t)], \tag{4}$$

where the time lag τ was taken as 2 days. The relative admittance for species m is then

$$Z_m(f) = w_{m0} + w_{m1}\,\mathrm{e}^{-2\pi i f\tau}, \tag{5}$$

the figures from which appear in the tables, except for species 3, whose tides were insignificantly small in most cases.

The harmonic constants listed in tables 2 to 4 may be considered the most reliable to date for these places, being derived from the longest available series by the most modern and precise

† The real part of a complex tidal synthesis is the usual 'predicted' tide; the imaginary part has the phases advanced by $\frac{1}{2}\pi$.

TABLE 3

Station: Isla de Trindade. 32 days, 21.1 May to 21.1 June 1961.
Reference: tide synthesis for Ascension Island (appendix C).

admittances (station/reference). intervals 1 c/m (0.036611 c/d)					principal harmonic constituents				
						station		reference	
c/d	real	imag.	R	$\phi°$	c/d	H/mm	$G°$	H/mm	$G°$
0.8929346	2.0212	2.1877	2.9785	47.27	(Q_1) 0.8932441	27	97.37	9	144.57
0.9295357	1.6210	1.4207	2.1555	41.23	O_1 0.9295357	55	154.79	26	196.02
0.9661368	0.9219	0.9111	1.2961	44.66					
					(P_1) 0.9972621	12	242.81	15	318.11
1.0027379	0.0692	0.7647	0.7678	84.83	K_1 1.0027379	38	240.58	50	324.41
1.0393390	−0.7598	1.0121	1.2656	126.90					
recorded variance 2662 mm²									
residual variance 427 mm²									
1.8590714	0.5335	−0.9091	1.0541	300.41					
1.8956725	0.6451	−0.6963	0.9492	312.81	(N_2) 1.8959820	70	208.60	74	161.53
1.9322736	0.8394	−0.5552	1.0064	326.52	M_2 1.9322736	331	210.30	328	176.82
1.9688747	1.0763	−0.5150	1.1931	334.43					
					(S_2) 2.0000000	170	220.00	122	196.00
2.0054758	1.3063	−0.5841	1.4310	335.91	K_2 2.0054758	50	222.47	35	198.38
recorded variance 68 502 mm²									
residual variance 3247 mm²									

TABLE 4

Station: Tristan de Cunha Island. 15 days, 6.0 to 21.0 March 1968.
Reference: tide synthesis for Ascension Island (appendix C).

admittances (station/reference). intervals 1 c/m (0.0366011 c/d)					principal harmonic constituents				
						station		reference	
c/d	real	imag.	R	$\phi°$	c/d	H/mm	$G°$	H/mm	$G°$
0.8929346	0.0872	0.7079	0.7132	82.98	(Q_1) 0.8932441	6	61.6	9	144.57
0.9295357	0.0694	0.4772	0.4822	81.72	O_1 0.9295357	12	114.3	26	196.02
0.9661368	−0.0488	0.2784	0.2826	99.95					
					(P_1) 0.9972621	4	176.3	15	318.11
1.0027379	−0.2431	0.1527	0.2871	147.86	K_1 1.0027379	14	177.6	50	324.41
1.0393390	−0.4729	0.1264	0.4895	165.04					
recorded variance 576 mm²									
residual variance 336 mm²									
1.8590714	−0.7553	0.2878	0.8083	159.14					
1.8956725	−0.7047	0.2422	0.7451	161.03	(N_2) 1.8959820	55	0.5	74	161.53
1.9322736	−0.6795	0.1789	0.7027	165.25	M_2 1.9322736	231	11.6	328	176.82
1.9688747	−0.6851	0.1110	0.6941	170.80					
					(S_2) 2.0000000	87	20.8	122	196.00
2.0054758	−0.7203	0.0526	0.7222	175.83	K_2 2.0054758	25	22.6	35	198.38
recorded variance 35 909 mm²									
residual variance 127 mm²									

methods. The figures for M_2 and S_2 do not differ greatly from other published estimates,† but there are considerable differences between the small diurnal constants and such figures as are available for comparison, as would be expected.

(*d*) *Have the St Helena tides changed in two centuries?*

The tide pole readings taken at Jamestown by Nevil Maskelyne (1762*b*) with the assistance of Charles Mason may not at first sight seem very promising material for comparison with modern

† See footnote on p. 613 about M_2 at Ascension.

data. But on reading Maskelyne's text, one realizes that the measurements were made with all the care and precision one should expect from leading astronomers of the day. Each sea level was the mean of up to 100 or more observations at different states of the swell over several minutes, and recorded against the mean time to the nearest $\frac{1}{4}$ min. Although tending to be clustered around daylight high and low water, intermediate readings were frequent and sometimes covered 24 h stretches. They span 40 days, from 12.3 November 1761 to 22.8 December, with only one serious lacuna, 3.3 to 5.7 December, when the pole was damaged by rollers† and plot with a smooth definition of the tide curve, small irregularities being compatible with atmospheric pressure variations and with our recent knowledge of medium-wave activity. Precision in timing could not be bettered,‡ since the work was done in conjunction with a study of the going of clocks in different latitudes (Mason 1762), requiring frequent astronomical checks. So the records are more than worthy of attention, and moreover provide a unique means of testing stability of the ocean tides over a period of almost precisely 208 years. Earlier tidal records of quality exist, for example the long series made at French ports during the early eighteenth century (Lalande 1781), but only at St Helena can one be sure of a complete absence of *local* changes in tide régime caused by varying shallows or man-made structures.

Before the data could be analysed, they had to be converted to metric units and Universal Time. The heights were recorded in units of three (English) inches, which I interpreted as 76.2 mm. *Apparent* times were recorded, that is, times reckoned from the local meridian transits of the Sun. To convert these to U.T. one has to add the time equivalent to the longitude west of Greenwich and the 'equation of time'. The equation of time in 1761 did not differ greatly from current years, but my calculations of it allowed for the known secular trends in obliquity of the ecliptic and in the eccentricity and mean anomaly of the Earth's orbit. I omitted only the planetary and lunar perturbations which would affect the results by less than 1 s.

To apply an equally precise correction for longitude is not so trivial as it may seem, for it requires the meridian of the observatory used for recording solar transits to within a mile or so. There have been at least five observatories§ on St Helena since Halley's celebrated visit of 1677. Historians of the island who touch upon the subject are agreed that Maskelyne's observatory (long since vanished) was situated high inland on the ridge behind Alarm House, whose longitude is 5° 42′.2. However, Maskelyne (1762*a*) had a clock going at an observatory 'near James's Fort, in a place 85′ above the level of the sea', at which he (and Waddington) used a transit telescope. Mason (1762) also 'set a clock a-going at St James's Fort', and observed transits there. Since Mason's clock observations cover the whole period of the tidal records, many of which were his own work by Maskelyne's acknowledgement (1762*b*, p. 588), it seems almost certain that the times were all reckoned from this place, whose longitude according to modern Admiralty charts is 5° 43′.2.

I calculated the correction for noon each day as described above, and applied this to all the recorded times for that day. Values of the correction at 5-day intervals are shown in table 5. I then analysed the corrected data by two methods, first by correlation with a tidal synthesis for Ascension, and secondly by a zero-lag correlation with a synthesis for St Helena itself, both tidal syntheses being computed for 1761 by use of the modern response weights. The calculations

† I was unable to detect any sensible change in datum after the pole was re-set.

‡ Except for a few misprints, e.g. where the readings 8 6 a.m. on 27 November and 4 37 p.m. on 20 December should obviously be 10 6 and 6 37 respectively.

§ I am indebted to Mr W. G. Tatham, Hon. Archivist to the St Helena Government for information on sites of observatories.

involved high precision lunar and solar ephemerides as described by Cartwright & Tayler (1971). These ephemerides made full allowance for secular trends in orbital constants over the span of two centuries, and also for the difference between Universal Time and Ephemeris Time, which was in fact only about 3 s in 1761 (Meeus 1962, p. 255). Figure 4 gives a general impression of some of the corrected data and a tidal synthesis derived from method 1.

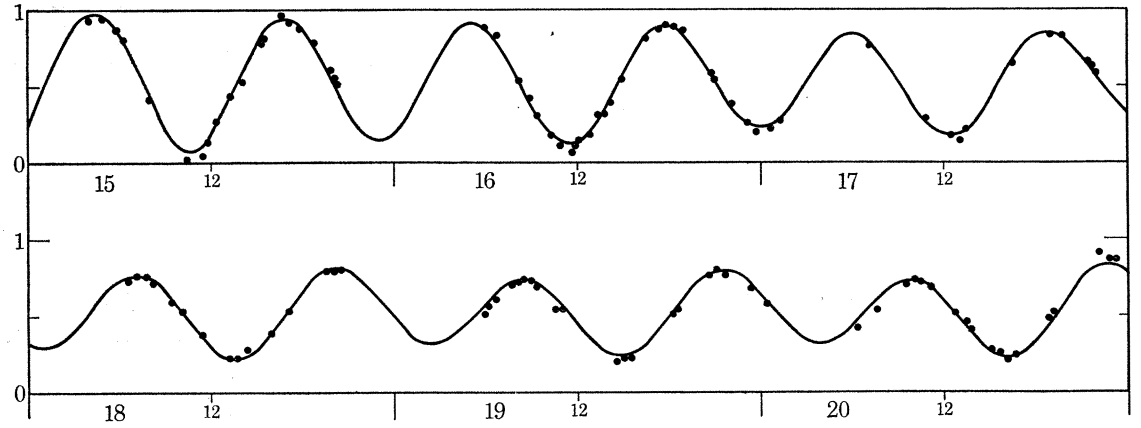

FIGURE 4. Sea-level observations by Maskelyne & Mason, converted to metres and universal time, for 15 to 20 November 1761, together with best tidal synthesis obtained by correlating the complete set of data with the Ascension Island reference. (Before and after the 6 days shown, the observations are mostly confined to daylight hours.)

TABLE 5. CORRECTIONS FROM APPARENT TO UNIVERSAL TIMES AT LONGITUDE 5° 43′.2 W

1761	Julian day	minutes
12.5 November	2364 568	+7.4
17.5	573	8.3
22.5	578	9.5
27.5	583	11.0
2.5 December	588	12.9
7.5	593	15.0
12.5	598	17.3
17.5	603	19.7
22.5	608	22.2

Method 1 is the same as that applied to the modern data, except for the calculation of the reference tides at arbitrary fractions of an hour, for which I used the interpolation procedure described in appendix B. The reference tide for Ascension is not necessarily the best synthesis for the real tide at Ascension in 1761, supposing that were known, but the best synthesis assuming the ocean admittance was the same then as in 1958/59. The admittance curves relative to Ascension derived from the ancient and modern data are compared in figure 5. In species 2 the curves are extremely close, especially in the region 1.9 to 2.0 c/d where the bulk of the energy is concentrated. At the frequency of M_2 (1.932 c/d) the amplitude is 0.98 times the modern value with 2.9° larger phase lead, while at S_2 (2.000 c/d) the trends are almost exactly reversed. The second method of analysis forces a constant transfer ratio, weighted in favour of the highest energy line at M_2, and in fact gives 0.984 with phase lead 2°.39, consistently with the figures just quoted from method 1. The differences are compatible with the noise variance as calculated from the modern data (table 2), and being reversed between M_2 and S_2, I consider them insignificant.

The differences in species 1 shown in figure 5 are much greater, but so is the noise: signal ratio. Now the residual variance quoted in table 2 is spread over a bandwith of 9 c/m, although much of

it is concentrated in 'cusps' about the major tidal lines O_1 and K_1 (e.g. as in figure 2*a*). If we assume the residual is effectively spread over a bandwidth of only 2 c/m, thus increasing the relative estimating variance by a factor of 4.5, this variance may be calculated as (cf. Munk & Cartwright 1966, p. 578)

$$\sigma^2 = \tfrac{1}{2}v_{\text{res}}/(v_{\text{tide}}\, w\, T),$$

where v_{res} and v_{tide} are the residual and tidal energies for the species, w is the assumed bandwidth of 2 c/m (0.073 c/d), and T is the duration of record analysed (39 days). With the given figures for species 1 we get a standard deviation of $\sigma = 0.10$ in amplitude, 5°.7 in phase. From figure 4, the amplitudes are in fact nearly equal at K_1 (1.003 c/d), though 0.83 at O_1 (0.930 c/d), but the ancient phase leads are consistently about 13° less at all frequencies. Method 2 gave 0.95 and −9°.1 as constant amplitude ratio and phase lead. Assuming the noise properties of the ancient data are about the same as the modern, we thus have some grounds for suspecting a genuine increase in diurnal phase lead by some 5° per century.

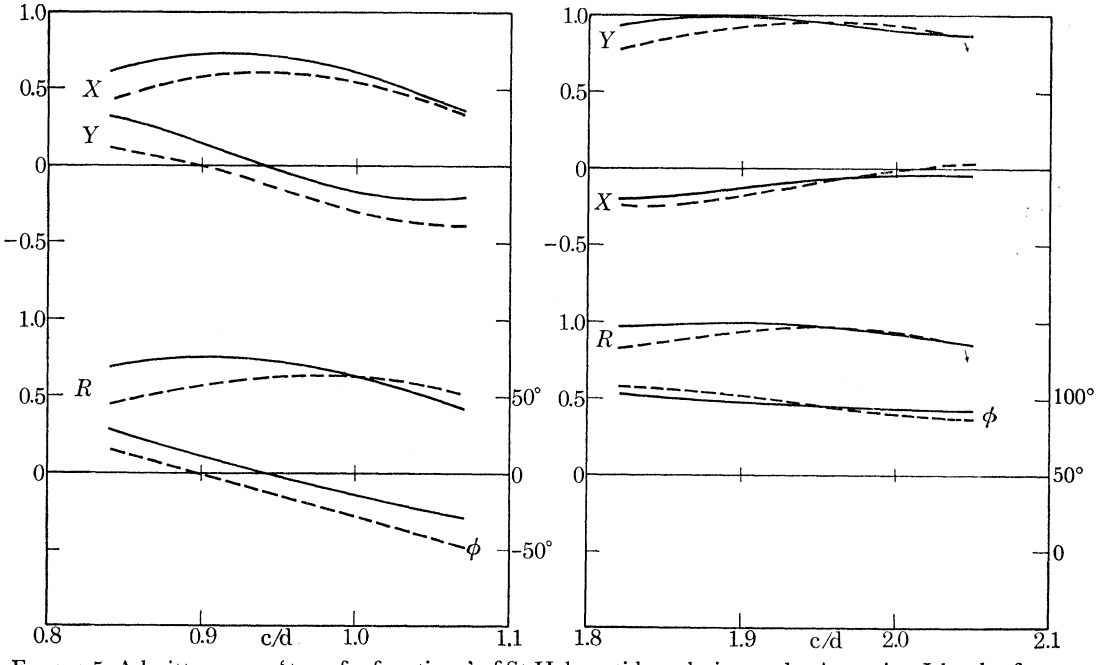

FIGURE 5. Admittances or 'transfer functions' of St Helena tides relative to the Ascension Island reference, based on 1969 data (full lines), and on the 1761 data (broken lines).

This result is consistent with the hypothesis that the diurnal tides in the Atlantic are in an unstable mode of oscillation, as suggested by the extraordinarily large phase change with frequency present in most of the eastern records, particularly in the north, and rapid differences in character from east to west. The association between large phase changes and oceanic 'Q-factor' has recently been analysed by Garrett & Munk (1971). By contrast, the species 2 admittances are everywhere much better behaved and may be considered more stable despite their large magnification in parts of this ocean. A secular trend in admittance does of course imply a change in some physical characteristics of the ocean as a whole. A possible mechanism is the steady increase in temperature from the 'Little Ice Age' of 1550 to 1850 (Lamb 1964) to the present day, associated with a recession of the polar ice boundaries and the raising of sea level affecting the co-oscillating tidal systems in shallow seas. The accompanying changes in thermocline structure also could affect the conversion from surface to internal tidal modes which may

play an important role in the ocean tidal dynamics (Munk 1968). However, with present knowledge, it would be hard to specify which of these physical changes would be most likely to modify the diurnal tides.

(*e*) *Cotidal maps*

How far do the tidal constants derived in (*c*) support the Pekeris–Accad amphidrome or the pictures given in other workers' cotidal maps? One cannot decide by a direct comparison, because interpretations as different as, for example, Pekeris–Accad and Hansen somehow contrive to be equally close to the island data, though none agrees perfectly. We therefore require an independent method for deducing the local cotidal map from the island data alone.

As a fair approximation, we may simply interpolate linearly the in-phase and quadrature components over the local space. That is for any harmonic constant (H, G) we may assign complex constants such that

$$H e^{iG} = Ax + By + C, \tag{6}$$

where x and y are quasi-Cartesian coordinates. In general, almost any set of numbers A, B, C will determine a family of straight cophase lines and elliptical coamplitude lines centred on an amphidrome $(Ax + By + C = 0)$, but the amphidrome may be outside the local area of validity. Fitting such constants exactly for M_2 at various triads selected from the four islands always gave positive amphidromes in the area, but at various places and not usually matching the constants at the fourth island very convincingly. I therefore compromised by satisfying (6) in a least-squares sense with squared residual at each island weighted by the number of days of record used to determine its tidal constants.† The resulting cotidal map for M_2 is drawn in figure 6*b* with the label 'Geometric'. It is fairly similar to the Pekeris–Accad map reproduced to its right, except that the 'geometric' amphidrome is farther south. Here, and in other parts of the world oceans, Pekeris & Accad show cophase lines consistently out by about 30°, possibly due to oversimplification of the role of friction in their model.

The least satisfactory feature of the 'geometric' map is that it does not necessarily satisfy the tidal dynamics. I therefore investigated another approach whereby the map is forced to satisfy Laplace's tidal equations (with allowance for the Earth tide), but with the simplifying assumptions of constant ocean depth and infinitely remote continental boundaries. Professor M. S. Longuet-Higgins has pointed out (private communication) that these assumptions are very dubious in the present application. However, they give rise to a tractable set of wave functions which satisfy the dynamical equations over a large part of the area, and an interpolation to the data in terms of them should, in the author's opinion, at least be more realistic than the linear form (6), even though the results cannot be claimed to be definitive. The situation here is complementary to the straight shelf boundary, semi-infinite ocean studied by Munk *et al.* (1970)—referred to hereinafter as M.S.W.

The area covered is too wide to ignore the variation of the Coriolis parameter as M.S.W. did, but we shall restrict the variation to being linear, (the 'β-plane' convention). Consider a β-plane with distance coordinates x (west) and y (south), both with origin at latitude $\theta = \theta_0 = -20°$, longitude $\lambda = \lambda_0 = 15°$. That is

$$\left.\begin{aligned} x &= a(\lambda - \lambda_0)\cos\theta, \\ y &= -a(\theta - \theta_0), \end{aligned}\right\} \tag{7}$$

† This weighting virtually assumes that the residual errors are due to sampling errors in the time series analysis, which is not entirely true, but it serves as a useful working rule which keeps the remote Tristan data fairly insignificant without ignoring the island altogether.

where a is the Earth's mean radius. Let ζ be the sea level *relative to the Earth's crust*, as measured by a tide gauge. Then, neglecting the small phase lag between the Earth-tide and the gravitational potential, Laplace's tidal equations may be applied directly with ζ as height variable, provided the forcing function is multiplied by the Love-number factor $(1+k-h) = 0.70$ (Proudman 1928; Grace 1930; M.S.W., pp. 182–183). Eliminating the currents from these familiar equations, we then obtain the following relation to be satisfied by ζ alone in water of depth $h(x, y)$ (Rhines 1969):

$$(h\zeta_x)_x + (h\zeta_y)_y + \frac{f}{\mathrm{i}\sigma}(h_y\zeta_x - h_x\zeta_y) + \frac{\beta h}{\sigma^2 - f^2}\left[\frac{\sigma^2+f^2}{\mathrm{i}\sigma}\zeta_x + 2f\zeta_y\right] + \frac{\sigma^2-f^2}{g}\zeta$$
$$= (h\bar{\zeta}_x)_x + (h\bar{\zeta}_y)_y + \frac{f}{\mathrm{i}\sigma}(h_y\bar{\zeta}_x - h_x\bar{\zeta}_y) + \frac{\beta h}{\sigma^2 - f^2}\left[\frac{\sigma^2+f^2}{\mathrm{i}\sigma}\bar{\zeta}_x + 2f\bar{\zeta}_y\right], \qquad (8)$$

in which $\bar{\zeta} = 0.70\times$ the equilibrium tide, the Coriolis factor is taken to be $f = f_0 + \beta y$, $(f_0, \beta < 0)$, and a time factor $\mathrm{e}^{-\mathrm{i}\sigma t}$ is understood.

As is usual, we first define a wave forced by the tidal potential with yielding crust, and then search for one or more free wave solutions to fit the observed constants less those of the forced wave. For the forced wave, we put

$$\bar{\zeta} = R(y)\,\mathrm{e}^{\mathrm{i}(\kappa x + m\lambda_0)},$$

where m is the tidal species and $\kappa = m/(a\cos\theta_0)$. Then with h uniform and scaling with respect to f (8) gives

$$\zeta = S(y)\,\mathrm{e}^{\mathrm{i}(\kappa x + m\lambda_0)},$$

where

$$\left.\begin{aligned} S_{yy} + \frac{2\beta'}{\omega^2-1}S_y + \left[(\omega^2-1)\gamma^2 - \kappa^2 + \frac{\beta'\kappa}{\omega}\frac{\omega^2+1}{\omega^2-1}\right]S = R_{yy} + \frac{2\beta'}{\omega^2-1}R_y + \left[-\kappa^2 + \frac{\beta'\kappa}{\omega}\frac{\omega^2+1}{\omega^2-1}\right]R, \\ \omega = \sigma/f, \quad \beta' = \beta/f > 0, \quad \gamma^{-2} = gh/f^2. \end{aligned}\right\} \qquad (9)$$

We also have (in millimetre units)

$$R(y) = -100\sin 2(y/a - \theta_0) \quad \text{for} \quad K_1$$

or

$$+171\{\tfrac{1}{2} + \tfrac{1}{2}\cos 2(y/a - \theta_0)\} \quad \text{for} \quad M_2,$$

and simple replacement of constants for O_1 or S_2, so that the solution $S(y)$ is obtained straightforwardly from the solutions of (9) for $R(y) = 1$ and $R(y) = \mathrm{e}^{2\mathrm{i}y/a}$ respectively. In M.S.W., the 'forced wave' was further modified (apart from the necessities of shelf geometry) by adding a free wave which renders the combined velocity normal to the coast zero. In the present case, I do not refer to either the African or the Brazilian coast, so no such adjustment is necessary.

The component amplitudes of the Earth tide-forced waves are included in tables 6. Their magnitudes are comparable with the island H values. The forced tides of species 2 are inverted with respect to the equilibrium tide, because of the size of the factor $\omega^2\gamma^2$ in (9). In species 1 they are not reversed, but still appear with negative amplitudes because of the sign of $R(y)$ in the southern hemisphere. We search for *free* waves of the form

$$\zeta = C\,\mathrm{e}^{\mathrm{i}(\kappa x + \mu y)}. \qquad (10)$$

With the forcing terms set equal to zero, (9) then gives

$$\kappa^2 + \mu^2 - \beta'\{\kappa(\omega^2+1) + 2\mathrm{i}\mu\}(\omega^2-1)^{-1} - \gamma^2(\omega^2-1) = 0. \qquad (11)$$

The imaginary i in the fourth term of (11) prevents a solution (10) with purely real wavenumbers, but with κ real and $\mu = \mu' + \mathrm{i}\mu''$, solutions occur for which either $\mu' = 0$ (a case I ignore) or $\mu'' = \beta'(\omega^2-1)^{-1}$. We thus have the solutions of form

$$\zeta = C\,\mathrm{e}^{-\beta' y/(\omega^2-1)}\,\mathrm{e}^{\mathrm{i}(\kappa x + \mu' y)}, \qquad (12)$$

PHILOSOPHICAL TRANSACTIONS OF THE ROYAL SOCIETY A MATHEMATICAL, PHYSICAL & ENGINEERING SCIENCES

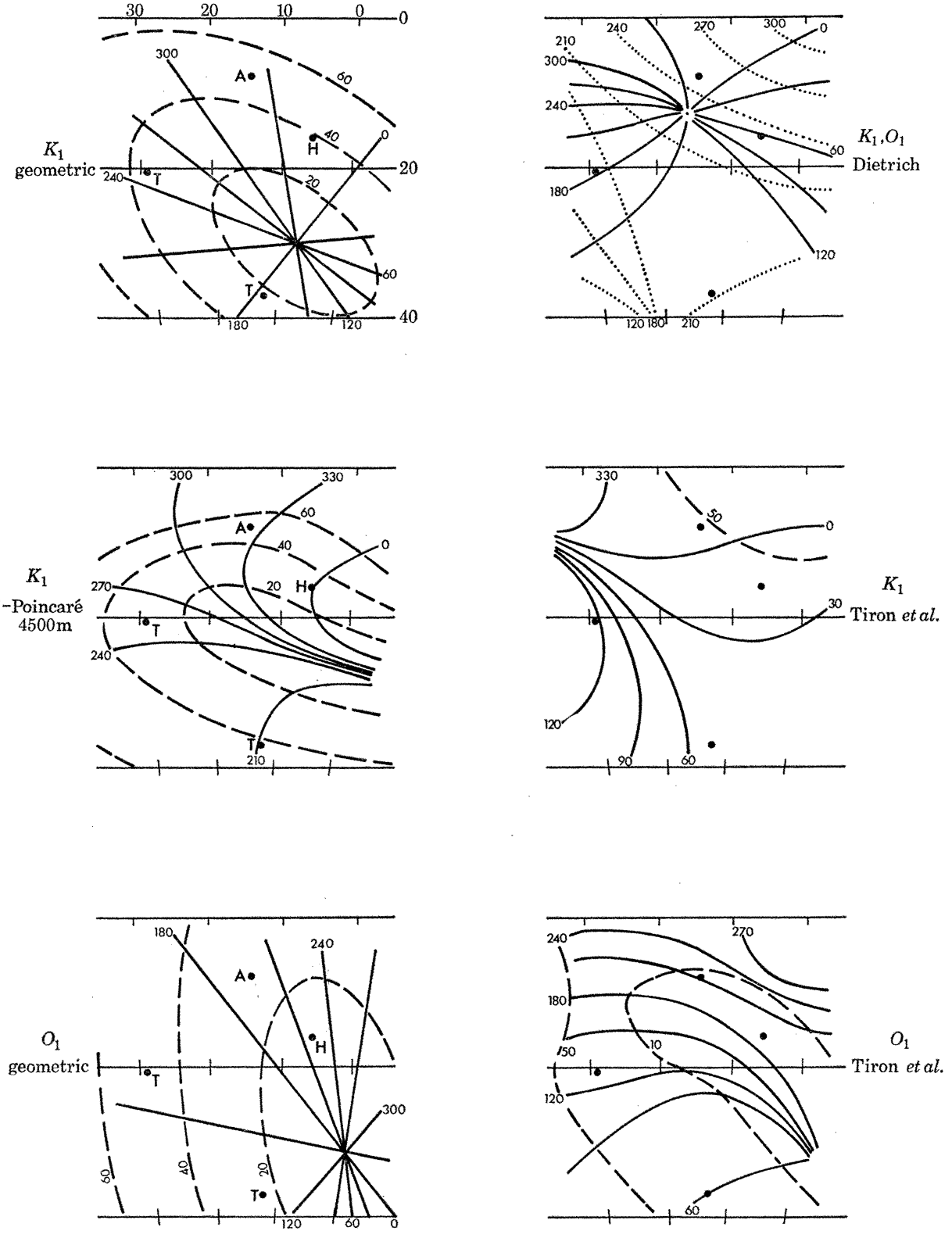

FIGURE 6 (*a*). Cotidal maps for diurnal constituents on β-plane; left, from island data by methods described in text; right, reproduced from the world maps of the authors cited. Full lines are cophase-lag in degrees, broken lines are co-amplitude (half corange) in millimetres. Dotted lines in top right are Dietrich's cophase lines for O_1. Larger numbers in top left diagram give west longitude and south latitude. Lettered circles indicate the four islands concerned.

PHILOSOPHICAL TRANSACTIONS OF THE ROYAL SOCIETY A MATHEMATICAL, PHYSICAL & ENGINEERING SCIENCES

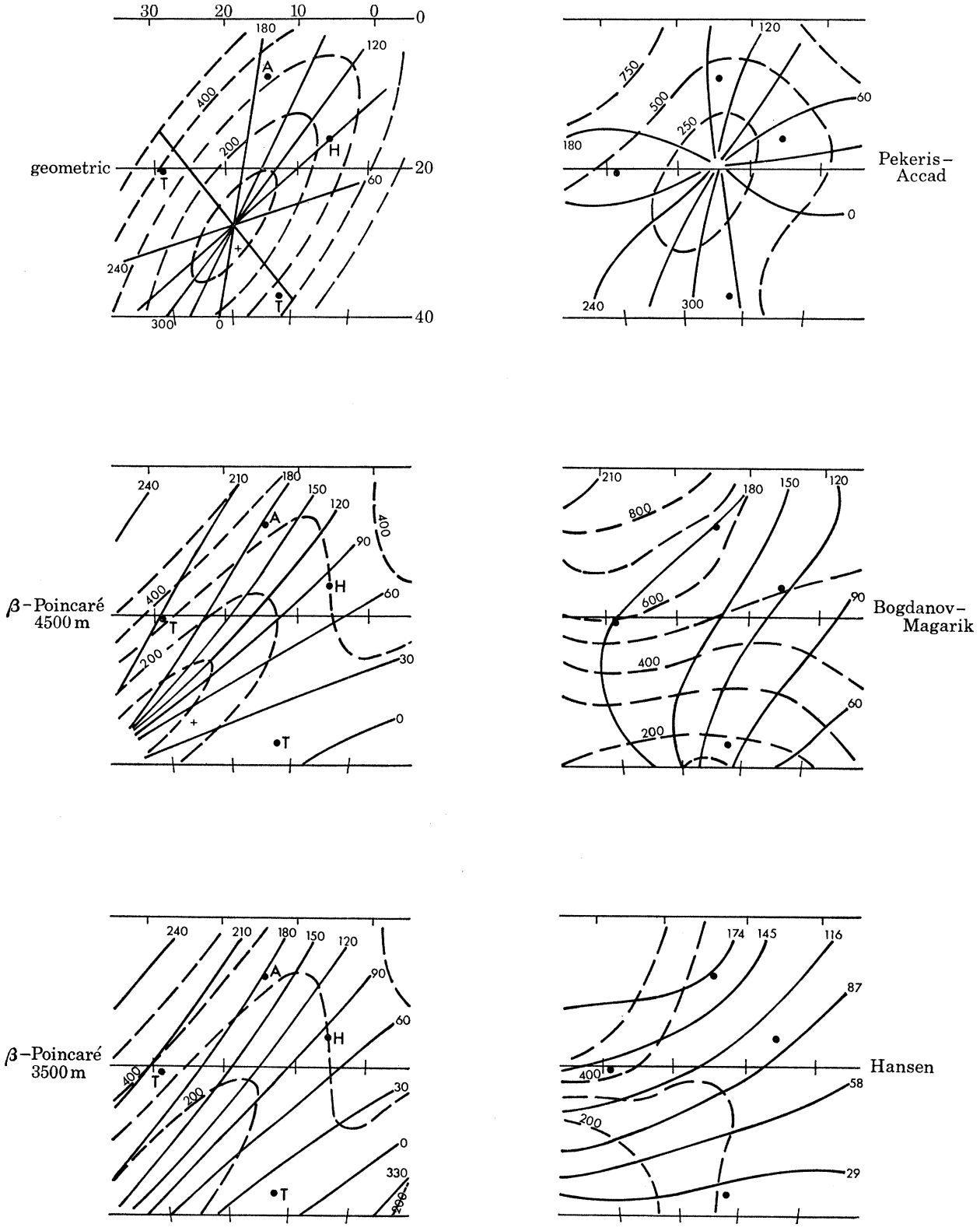

FIGURE 6 (*b*). As (*a*) for the M_2 tidal constituents. Crosses in upper two left hand maps show the positions of the corresponding amphidromes for S_2.

PHILOSOPHICAL TRANSACTIONS OF THE ROYAL SOCIETY A MATHEMATICAL, PHYSICAL & ENGINEERING SCIENCES

which may be termed 'β-Poincaré' waves, being essentially trigonometric but with exponential decay away from the Equator. For tides of species 2 the exponential factor is rather mild, but for species 1 and $\theta_0 = -20°$, it attenuates the amplitudes by 1.5 in 10 degrees, approximating to the fact that in water of uniform depth such waves are strictly confined to the equatorial zone for which $|\omega| > 1$, that is for latitudes within about 30°. With condition (12), one finds that the locus of all possible real wavenumbers in the (κ, μ') plane is a circle with centre on the positive κ-axis at

$$\kappa_0 = \tfrac{1}{2}\beta'(\omega^2+1)\,(\omega^2-1)^{-1}, \tag{13}$$

and radius

$$\rho = \sqrt{[\beta'^2(\tfrac{1}{4}(\omega^2+1)^2-1)\,(\omega^2-1)^{-2}+\gamma^2(\omega^2-1)]}. \tag{14}$$

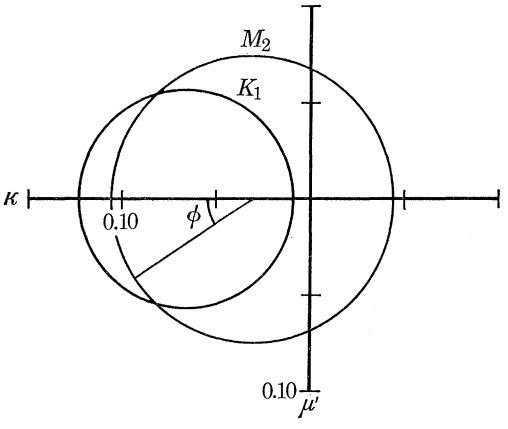

FIGURE 7. Wavenumber circles for free β-Poincaré waves in 4500 m depth with frequencies corresponding to the K_1 and M_2 tides. Units are radians per terrestial degree.

Figure 7 shows typical wavenumber circles, for M_2, which includes the origin, and for K_1, which does not.

I fitted pairs of β-Poincaré waves to the observed data as follows. Let $\phi = \phi_1$ and ϕ_2 be any two angles (ϕ as in figure 7), and let

$$\left.\begin{aligned} \zeta_n(x,y) &= C_n\,\mathrm{e}^{-\beta' y/(\omega^2-1)}\,\mathrm{e}^{\mathrm{i}(\kappa_n x+\mu'_n y)} \\ \text{where}\quad \kappa_n &= \kappa_0+\rho\cos\phi_n \\ \text{and}\quad \mu'_n &= \rho\sin\phi_n \end{aligned}\right\} \quad n = 1, 2. \tag{15}$$

Further, let $V(\phi_1, \phi_2)$ be the minimum value of

$$\sum_p T_p\,|\zeta_1(x_p,y_p)+\zeta_2(x_p,y_p)-(H_p\,\mathrm{e}^{\mathrm{i}G_p}-H'_p\,\mathrm{e}^{\mathrm{i}G'_p})|^2 \tag{16}$$

with respect to C_1 and C_2, where the summation is over the four places p, T_p are the weighting factors mentioned in the 'geometric' case, and H'_p, G'_p are the constants appropriate to the forced wave. I first computed $V(\phi_1, \phi_2)$ for all combinations $0 \leqslant \phi_1 < \phi_2 \leqslant 360°$ in steps of 15°. The results showed that V had just one minimum in space, and I located this by further computations at 1° steps over the critical ranges. Contours of the quantity $1 - V/V_0$ (where V_0 is the value of (16) when $C_1 = 0 = C_2$) for M_2 with $h = 4500$ m are plotted in figure 8 over all relevant (because of symmetry) values of ϕ_1, ϕ_2. Their greatest value of 0.997, corresponding to minimum V, represents a very satisfactory fit to the data. The analogous quantity when only one wave ζ_1 is allowed is also plotted in figure 8, and shows a significantly lower maximum of 0.803. All wave amplitudes involved are listed in tables 6A and 6B.

The map corresponding to the solutions just described is shown mid-left in figure 6*b*. The amphidrome is now just off the southwest corner of the β-plane, rather closer to that obtained by Bogdanov & Magarik (1967), reproduced to the right, although the general pattern of co-amplitude lines still bears more resemblance to the map of Pekeris and Accad than to any other. The corresponding map for S_2 does bring the amphidrome into the picture, as shown by the cross; it is otherwise similar to the M_2 map and is not reproduced.

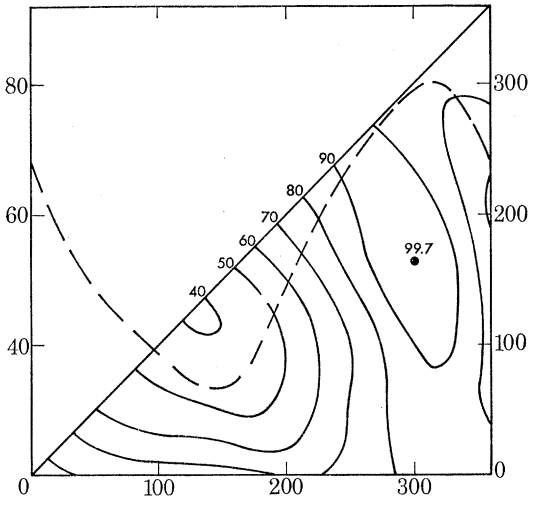

FIGURE 8. Contours of percentage fit $100(1-V/V_0)$ to island constants for pair of β-Poincaré waves with angle parameters ϕ_1 and ϕ_2 in degrees, calculated for the M_2 frequency with 4500 m depth. Broken curve and left hand scale shows corresponding values for a single wave ϕ_1.

The assumed depth of 4500 m is typical of the Brazilian and Angolan Basins which occupy the greater part of the area, but the mid-Atlantic ridge is considerably shallower, typically about 2500 m at its summit. I therefore carried out similar computations with a mean depth of 3500 m, and the result is shown at the bottom left of figure 6*b*. Evidently, the general character is not greatly altered even though the forced wave amplitudes (table 6B) are almost halved, but there is a slightly closer resemblance to Hansen's (1952) map, bottom right, which does not show any amphidrome south of the Equator. Hendershott's (1970) map, not reproduced here, is similar to Hansen's in this area. Although these results suggest that variations in depth of order 1000 m are unimportant, a computation which allowed for a north–south ridge of triangular cross-section, as investigated by Rhines (1969) at very low frequencies, may show distinct anomalies akin to the 'double-Kelvin' waves of Longuet-Higgins (1968). But if the ridge were a critical feature we should also have to allow for the normal Kelvin waves (imaginary κ) associated with the two coastlines. To involve these would introduce complications outside the scope of this paper.

Turning now to the diurnal tides, the 'geometric' map for K_1 (figure 6*a*, upper left) reproduces a central amphidrome with negative rotation (contra solem), as in Dietrich's (1944) map, top right, but further to the southeast. Dietrich's empirical maps do not include amplitudes, and I have reproduced his cophase lines for O_1 on the same map. The only workers to attempt complete diurnal maps for the Atlantic Ocean (albeit with very sparse coamplitude contours) appear to be Tiron *et al.* (1967); see figure 6*a* mid and bottom right. Both maps differ considerably from Dietrich's and from mine. The β-Poincaré synthesis again fits the island data very well, with $1-V/V_0 = 0.993$ (0.959 for a single wave). The map for K_1, mid left, sends the amphidrome off to

the east. The interpretation of Tiron *et al.* suggests an amphidrome to the west, but this is a virtual one, associated with the coastal system. As mentioned in § 3 (*a*), they do show an amphidrome for K_1 southeast of Simons Bay, in keeping with the diurnal node present in the data there, and perhaps also with the β-Poincaré map. The solutions for $h = 3500$ m (table 6A) differ only slightly, because the term $\gamma^2\omega^2$ is much less important than in species 2.

TABLE 6A. FORCED AND FREE WAVE CONSTANTS, SPECIES 1

(Amplitudes in millimetres, wavenumbers in radians/terrestial degree.)

Constituent: K_1 $\omega = -1.4618$ $h = 3500$ m
Forced wave: $S(y) = -92\cos(2y/a) - 75\sin(2y/a)$

Island	$H\cos G$	$H\sin G$	$H'\cos G'$	$H'\sin G'$	'free' residual	
Ascension	41	−28	−51	−13	92	−15
St Helena	29	−10	−80	−8	109	−2
Trindade	−19	−33	−81	−46	62	12
Tristan da Cunha	−14	1	−115	−25	101	26

Free waves: $\kappa_0 = 0.0662$ $\rho = 0.0602$ $\beta'/(\omega^2-1) = 0.0422$ $1 - V/V_0 = 0.9937$

n	ϕ_n	κ_n	μ'_n	wavelength	direction	Re (C_n)	Im (C_n)
1	175.0	0.0062	0.0052	772°.6	229°.9	108	−57
2	230.0	0.0275	−0.0461	117°.1	329°.2	−14	71

Constituent: K_1 $\omega = -1.4618$ $h = 4500$ m
Forced wave: $S(y) = -85\cos(2y/a) - 76\sin(2y/a)$

Island	$H\cos G$	$H\sin G$	$H'\cos G'$	$H'\sin G'$	'free' residual	
Ascension	41	−28	−45	−11	86	−17
St Helena	29	−10	−73	−7	102	−3
Trindade	−19	−33	−75	−42	56	9
Tristan da Cunha	−14	1	−110	−24	96	25

Free waves: $\kappa_0 = 0.0662$ $\rho = 0.0582$ $\beta'/(\omega^2-1) = 0.0422$ $1 - V/V_0 = 0.9934$

n	ϕ_n	κ_n	μ'_n	wavelength	direction	Re (C_n)	Im (C_n)
1	177°.3	0.0080	0.0027	745°.2	251°.0	107	−59
2	231°.0	0.0295	−0.0453	116°.3	326°.9	−20	72

Constituent: O_1 $\omega = -1.3551$ $h = 4500$ m
Forced wave: $S(y) = -54\cos(2y/a) - 54\sin(2y/a)$

Island	$H\cos G$	$H\sin G$	$H'\cos G'$	$H'\sin G'$	'free' residual	
Ascension	−24	−7	−26	−7	1	0
St Helena	−19	−4	−45	−5	27	0
Trindade	−50	23	−48	−27	−2	50
Tristan da Cunha	−5	11	−73	−16	68	27

Free waves: $\kappa_0 = 0.0813$ $\rho = 0.0625$ $\beta'/(\omega^2-1) = 0.0573$ $1 - V/V_0 = 0.8078$

n	ϕ_n	κ_n	μ'_n	wavelength	direction	Re (C_n)	Im (C_n)
1	81°.7	0.0903	0.0619	57°.4	235°.6	35	−8
2	244°.1	0.0540	−0.0562	80°.6	316°.2	4	36

The β-Poincaré fit for O_1 was unusually poor, with $1 - V/V_0 = 0.808$. We see from table 6A that the forced wave for O_1 leaves very small residuals at Ascension and St Helena and large residuals at Trindade and Tristan. Such a situation is difficult to fit with free waves of type (12) because of the exponential factor which reduces the amplitudes to the south. Kelvin waves progressing up the Brazilian coast may also play an important role, especially at Trindade, where the O_1 constituent is enhanced relative to K_1; Vitoria at the same latitude has $H = 88$ mm for O_1, 52 mm for K_1, (I.H.B. sheet 1047). However, the very large free wavelength at ϕ_1 for K_1 suggests how a

Kelvin wave may be simulated by a Poincaré wave over a limited area. The fundamental cause of the difficulty is probably the fact of Tristan at latitude $-37°$ being strictly outside the zone of validity of the free wave model for diurnal tides. Variations in depth again no doubt confuse the simplified model. The fit being dubious, I show only the 'geometric' map for O_1, which in fact agrees with Tiron *et al.* in the position and sense of its amphidrome. Dietrich's O_1 amplitude is considerably further to the southwest.

TABLE 6B. FORCED AND FREE WAVE CONSTANTS, SPECIES 2

(Amplitudes in millimetres, wavenumbers in radians/terrestial degree)

Constituent: M_2 $\omega = -2.8171$ $h = 3500$ m
Forced wave: $S(y) = -46 - 95\cos(2y/a) + 39\sin(2y/a)$

Island	$H\cos G$	$H\sin G$	$H'\cos G'$	$H'\sin G'$	'free' residual	
Ascension	−327	18	−131	−72	−197	90
St Helena	48	316	−143	−29	191	345
Trindade	−286	−167	−73	−120	−212	−47
Tristan da Cunha	226	46	−94	−43	320	90

Free waves: $\kappa_0 = 0.0309$ $\rho = 0.0845$ $\beta'/(\omega^2-1) = 0.0069$ $1 - V/V_0 = 0.9946$

n	ϕ_n	κ_n	μ'_n	wavelength	direction	Re (C_n)	Im (C_n)
1	170°.4	−0.0524	0.0141	115°.7	105°.0	116	−50
2	304°.6	0.0789	−0.0696	59°.7	311°.4	−94	308

Constituent: M_2 $\omega = -2.8171$ $h = 4500$ m
Forced wave: $S(y) = -71 - 189\cos(2y/a) + 45\sin(2y/a)$

Island	$H\cos G$	$H\sin G$	$H'\cos G'$	$H'\sin G'$	'free' residual	
Ascension	−327	18	−229	−126	−98	144
St Helena	48	316	−259	−52	307	369
Trindade	−286	−167	−135	−221	−151	54
Tristan da Cunha	226	46	−184	−84	410	131

Free waves: $\kappa_0 = 0.0309$ $\rho = 0.0759$ $\beta'/(\omega^2-1) = 0.0069$ $1 - V/V_0 = 0.9972$

n	ϕ_n	κ_n	μ'_n	wavelength	direction	Re (C_n)	Im (C_n)
1	163.1	−0.0417	0.0221	133°.2	117°.9	190	−51
2	299.5	0.0682	−0.0660	66°.2	314°.0	−32	347

Constituent: S_2 $\omega = -2.9158$ $h = 4500$ m
Forced wave: $S(y) = -28 - 66\cos(2y/a) + 23\sin(2y/a)$

Island	$H\cos G$	$H\sin G$	$H'\cos G'$	$H'\sin G'$	'free' residual	
Ascension	−117	−34	−86	−47	−32	13
St Helena	−25	109	−95	−19	69	128
Trindade	−130	−109	−49	−80	−82	−29
Tristan da Cunha	81	31	−64	−29	145	60

Free waves: $\kappa_0 = 0.0304$ $\rho = 0.0783$ $\beta'/(\omega^2-1) = 0.0064$ $1 - V/V_0 = 0.9927$

n	ϕ_n	κ_n	μ'_n	wavelength	direction	Re (C_n)	Im (C_n)
1	178°.7	−0.0479	0.0018	131°.1	92°.1	78	−27
2	298°.4	0.0676	−0.0689	65°.1	315°.5	−48	105

In summary, these cotidal maps emphasize even more than M.S.W. our unsatisfactory state of knowledge about the ocean tides. In this ocean area, amphidromes probably occur at all tidal frequencies, but estimates of their positions vary greatly according to whether one searches for them on a global scale without empirical data (Pekeris & Accad), by use of coastal data (all other authors cited), or from the central islands (β-Poincaré solutions). All the usual analytical methods are more or less suspect (Hendershott & Munk 1970), and this ocean seems a very suitable one for

testing improvements in realism, on account of its sensitivity. The island data provide new material for testing, but further measurements of pressure and currents† in the open ocean are also needed.

4. Swell waves

We were unable to achieve our main objective, to analyse 'rollers', because they never occurred during the period of our stay. A continual 'ground swell' was however always present, occasionally up to 0.5 m high at tripod (1) and with crests clearly visible (see figure 18, plate 13)—and this provided material for useful analysis. It is extremely likely that genuine 'rollers' merely consist of large amplitude swell, the sudden shoaling close to the island producing the sudden increase in height which gives the impression to local mariners of a disturbance 'arising from the depths of the ocean' (to quote one of them). If this is so, then our swell records are as good a sample of their essential characteristics as much larger waves would be.

The waves in James Bay are not of course entirely typical of the open sea, since that part of the shore line is very effectively sheltered from the continual southeast trade wind seas. Similarly, one would not sense any *swell* from the southeast quadrant, but swell from any other quarter would

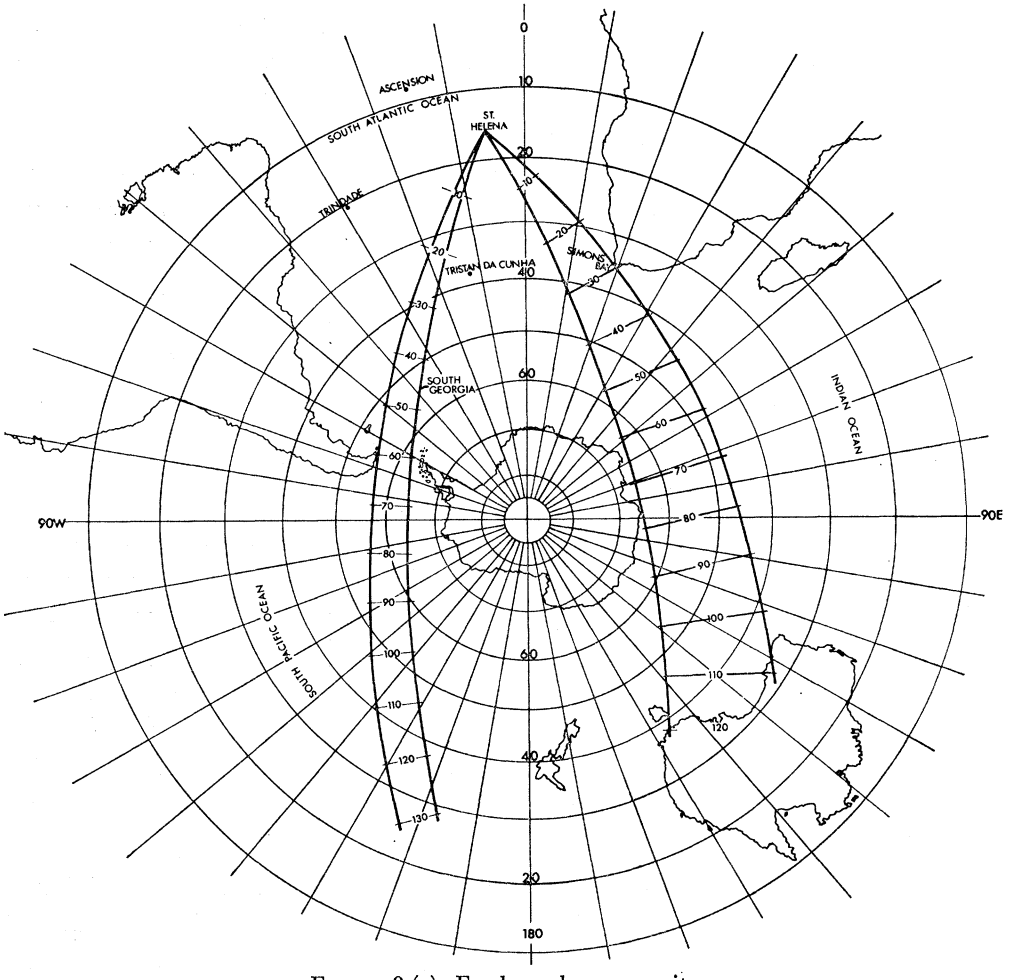

Figure 9 (*a*). For legend see opposite.

† Tidal current data from short records taken by the *Meteor* and other ships, quoted by Defant (1961, p. 493) are unlikely to be reliable in view of the low coherence between deep ocean tidal currents and pressures found by M.S.W.

FIGURE 18. View of swell off Thompsons Bay approaching from the southwest (left of picture) on 9 November about 16 h. The shorter waves in part of the foreground are due to scattering by an offshore islet.

(*Facing p.* 628)

PHILOSOPHICAL TRANSACTIONS OF THE ROYAL SOCIETY A MATHEMATICAL, PHYSICAL & ENGINEERING SCIENCES

be at least refracted into James Bay. As is well known, and best shown by Munk *et al.* (1963) and by Snodgrass *et al.* (1966), swell energy is propagated along great circles. The bounding great circles from St Helena tangential to the principal land masses are plotted in figure 9. Apart from the local ocean within 2000 km, James Bay is well exposed to a wide and stormy sector of the northwest Atlantic, the Argentine Basin, and a narrow pencil from the Pacific Ocean through Drake Passage. This pencil, limited by Cape Horn and South Georgia at 8° in azimuth, is interesting in that it provides the longest possible 'view', extending beyond the antipode north of the Marshall Isles to the Kuril island chain bounding the Sea of Okhotsk, some 215° distant.

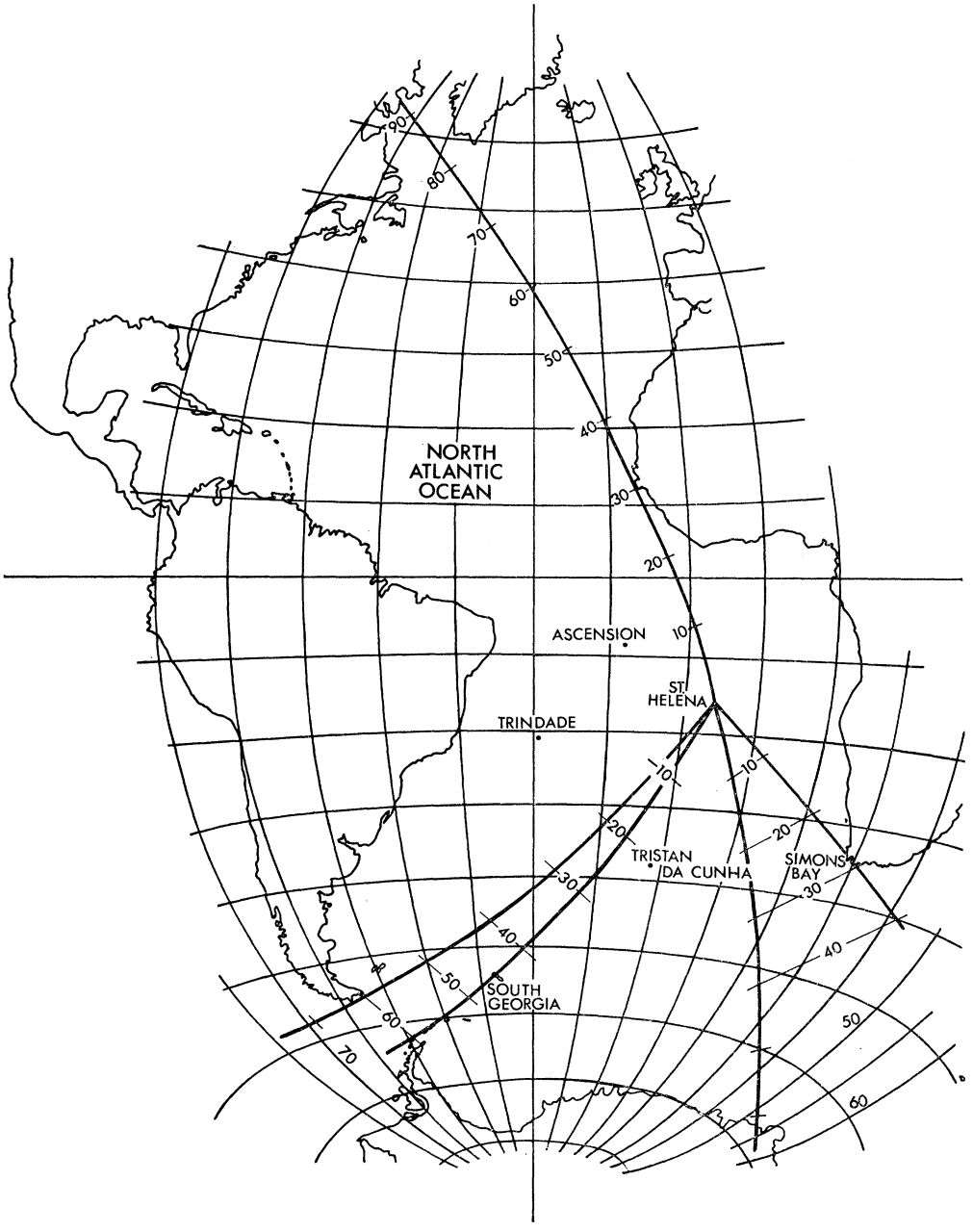

FIGURE 9(*a*), (*b*). Great circles through St Helena tangential to the continental land masses, with distances in terrestial degrees.

PHILOSOPHICAL TRANSACTIONS OF THE ROYAL SOCIETY A MATHEMATICAL, PHYSICAL & ENGINEERING SCIENCES

Along this route one might expect to receive swell from the tropical typhoon belt near Samoa; (like the St Helena rollers, typhoons are most common January to March), and possibly tsunamis from the seismically active Kuril region. The long-range pencil from Australia (20° in azimuth, 115° distant), through the southern Indian Ocean, where easterly winds are not common anyway, approaches on the windward side and does not concern us.

I computed energy spectra by standard procedures for all 69 of the 160 min swell records which were faultless or nearly so. The bandwidth was 1/320 Hz, so estimates of logarithmic spectral energy density have a standard error of 0.7 dB.† These estimates were compiled on a frequency/time diagram and from these the isopleths of energy density were plotted in figure 10, after the manner of and with the same units as Snodgrass *et al.* (1966). As with the results in that paper, the bulk of the energy lies within a band of 50 to 100 mHz ('periods' 20–10 s), leaving a fairly uniform trough at about −20 db in the band 10–40 mHz. Snodgrass *et al.* recorded peak energy levels over 20 db on frequent occasions at tropical islands in the Pacific. Figure 10 barely exceeds 5 dB twice, but the level would no doubt rise to 20 dB during a period of 'rollers'.

Despite the very low general energy level, the diagram shows several clear examples of the familiar sloping ridges from dispersive wave systems of distant origin. Since short wave energy at frequency f Hz spreads across the ocean at the group velocity $c_g = g/4\pi f$, it follows that the frequency of the energy peak from a source at distance Δ increases linearly at the rate $(g/4\pi\Delta)$ s^{-2}, and is measured at time Δ/c_g after its origin, as first demonstrated by Barber & Ursell (1948). Eight such events are identified in figure 10, marked by straight lines which if correctly drawn intersect the axis of zero frequency at the date of origin. On each line is written the corresponding source distance Δ in terrestial degrees, proportional to $(\mathrm{d}f/\mathrm{d}t)^{-1}$. I attempted to identify these with the dates and distances of strong winds in the right direction shown in the 12 h surface weather analyses for the southern hemisphere and the tropics published by the U.S. Weather Bureau and for the northwest Atlantic in the daily weather reports published by the British and Venezuelan meteorological authorities.

The two events at distances 129° and 130° are of special interest, because such distances exist only along the Drake Passage pencil to the central south Pacific. The earlier line suggests an origin about 17 to 18 October, the second 4 to 5 November as shown, both within a few degrees of the position 160° W, 25° S. Unfortunately, since the whole span of the pencil between here and Drake Passage is devoid of islands and has little shipping, weather analyses for this area can only be speculative. Depressions are indeed shown producing westerly winds in about the areas sought on 17 October and 4 November and at no other time, but they do not appear to be strong enough to produce the 40-knot or stronger winds necessary to generate 60 to 80 mHz waves.

The 84° distant source of 29 to 30 October produced the largest waves encountered. Views from the island's central peak and closer to the water line (figure 18) showed crests advancing from the southwest over Speery Ledge and into Thompson's Bay. This points again to the Drake Passage pencil, some 20° southwest of Chile, and we have corroboratory evidence for such a source in close east–west isobars with pressure increasing northwards by 4–5 mbar/deg (mbar = 10^2 Pa) covering a wide area west of the Passage in the maps for 30 October. The Argentinian weather map for noon 30 October in fact shows 45 knot westerly winds at Cape Horn itself, but suggests still stronger winds farther west. A similar weather situation occurred on 21 to 22 November when figure 10 gives a source distance of 83°. We did not observe any

† The reckoning is $10 \lg (1 + (320/9600)^{\frac{1}{2}}) = 0.72$.

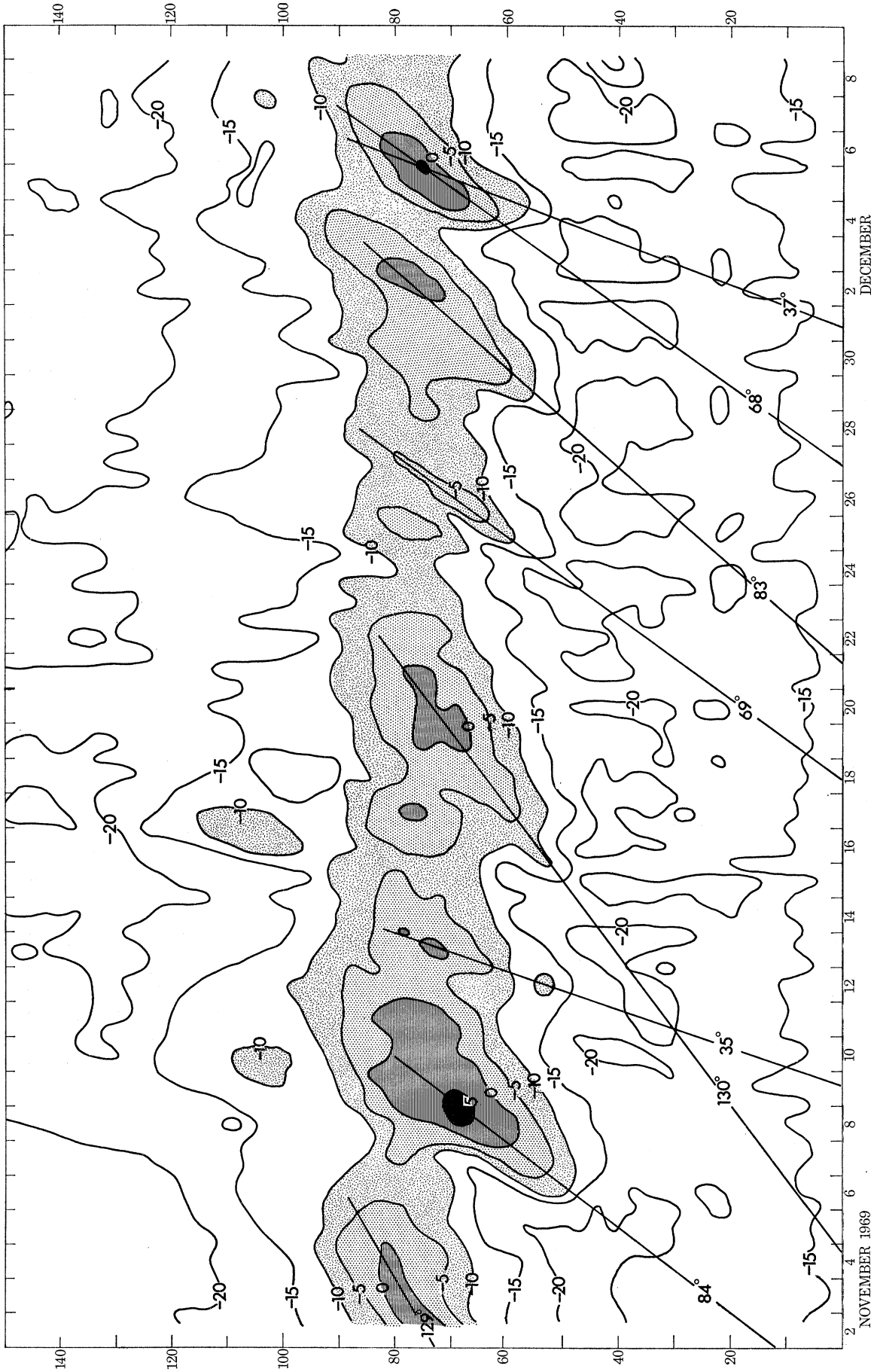

FIGURE 10. Contours of spectral energy density in decibels relative to 1 cm² (mHz)⁻¹ plotted for 12 h 160 min wave records. Numbers along ridge lines are calculated distances of storm events in terrestial degrees.

PHILOSOPHICAL TRANSACTIONS OF THE ROYAL SOCIETY A MATHEMATICAL, PHYSICAL & ENGINEERING SCIENCES

directional swell crests in early December, but the only other possible source area at this distance was the Labrador Sea, which had southerly winds at the dates concerned.

Another occasion when we observed the direction of swell was 5 December, when the crests were just discernible from a height to be approaching from the northwest. A small but intense depression with recorded 30 knot northwesterly winds† some 15° south of Newfoundland, 27 to 28 November, clearly accounts for the event shown. A similar depression with 40 knot (knot = 0.51 m/s) northwesterly winds occurred 18 to 19 November, accounting for the rather low ridge observed 24 to 26 November. The two ridge lines from sources 35° and 37° distant are less clearly defined, but appear to originate from depressions in the area of Tristan da Cunha and the Argentine Basin respectively.

As a final piece of information of more qualitative nature, a makeshift pneumatic wave recorder which we left at James Bay in the hope of recording 'rollers' during early 1970 had its airline ruptured at the first onset of such phenomena, about 3 January. Assuming a typical frequency of 70 mHz, this correlates convincingly with a wide area of northwesterly 40 knot winds east of Newfoundland reported in the British daily weather report for 26 December.

To summarize the conclusions, the low energy swell at St Helena is similar in character to swells recorded in other oceans, and like them originates from very distant storms. It is clear that swell from the Pacific Ocean can be sensed through the 8° pencil, but one would need a tropical typhoon to obtain reliable correlation with weather. We recorded only slight swells from the northwest Atlantic, but all the depressions responsible were minor ones. Major depressions in that area are common in the early months of the year, and could well be capable of producing a heavy swell in James Bay which could not be classed otherwise than as 'rollers'. In due course, we hope to obtain more extensive swell records from the island.

5. Trapped waves

(*a*) *Bathymetry*

The current edition of the Admiralty chart for St Helena shows most of its soundings close to the shoreline and only a few widely spaced values in the deeper water. In order to improve the bathymetry and to help our work on trapped waves, Commander J. Paton, R.N., agreed to spend a day taking H.M.S. *Vidal* on a pattern of soundings along the five radial lines shown in figure 1. The 1000 and 2000 fathom (fm = 1.83 m) contours shown in that figure were drawn very roughly from them.

The five new lines of soundings are plotted in greater detail in figure 11 against radial distance from their approximate focal point at 15° 58′ S, 5° 43′ W, in the centre of Sandy Bay Ridge. The contours are elongated over the first kilometre or so of depth, but thereafter the profiles intertwine, and on the whole they approximate to circular symmetry about as well as could be expected for a natural island. Note that there is no profile shown over Speery Ledge, whose 100 m contour probably extends farther south than is shown in figure 1, and could prove a considerable obstacle to higher order trapped waves. However, reducing the situation to the simplest shape which can be tractably analysed, the paraboloidal profile shown on the right of figure 11 seems to be a fair approximation. The depth h at radius r is of the form

$$h/h_1 = (r/r_1)^2 \quad (r_1 \leqslant r \leqslant r_2), \tag{17}$$

with $r_1 = 6$, $r_2 = 28$, $h_1 = 0.18$, $h_2 = h(r_2) = 3.92$ in kilometre units.

† Stronger winds are of course possible where there were no ships to record them.

PHILOSOPHICAL TRANSACTIONS OF THE ROYAL SOCIETY A MATHEMATICAL, PHYSICAL & ENGINEERING SCIENCES

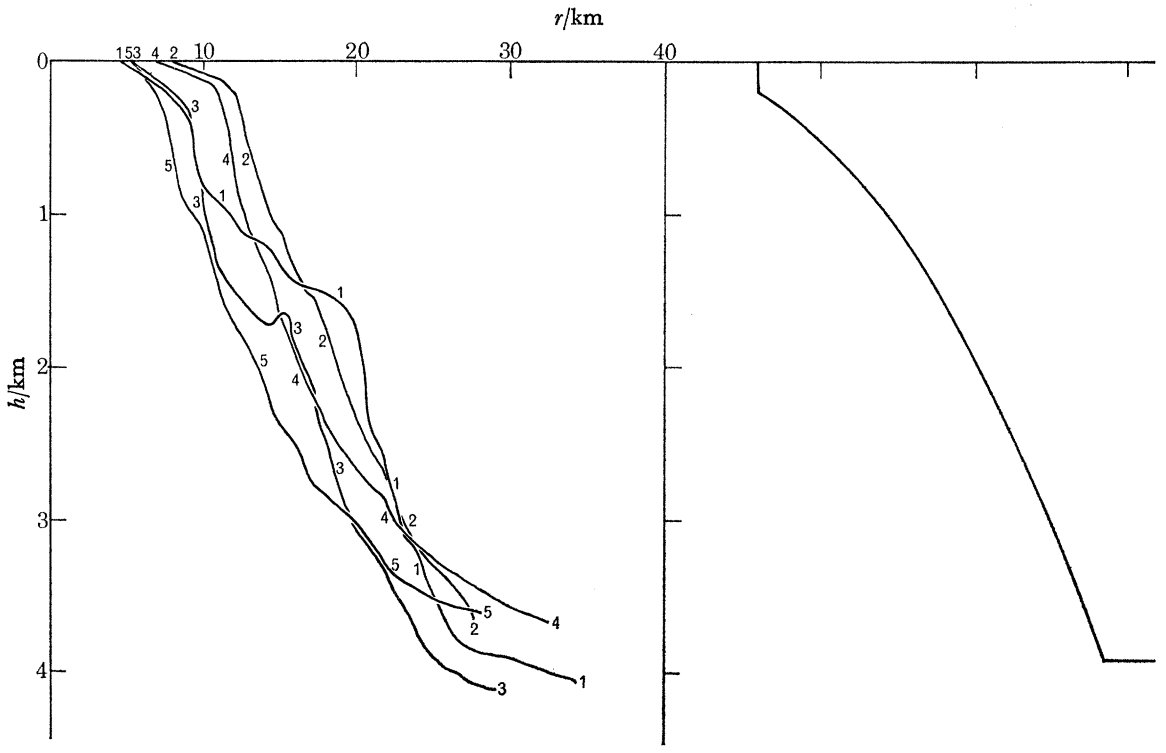

FIGURE 11. (Left). Depth traverses from soundings along radials 1–5 shown in figure 1. (Right) Cross-section of paraboloid used to calculate wave-trapping.

(b) *Theory*

With horizontal polar coordinates r and θ and frequencies ω very much greater than $(2\pi/$ pendulum day), so that geostrophic forces can be ignored, free waves of the form

$$\zeta(r, \theta, t) = F(r)\, e^{i(n\theta - \omega t)} \tag{18}$$

have to satisfy the condition $$F'' + \left(\frac{1}{r} + \frac{h'}{h}\right)F' + \left(\frac{\omega^2}{gh} - \frac{n^2}{r^2}\right)F = 0, \tag{19}$$

where the prime represents a derivative with respect to r (Longuet-Higgins 1967, p. 789). Two forms of depth profile $h(r)$ give reasonably tractable solutions of (19), namely

$$\left.\begin{aligned} h(r) &= h_2 = \text{constant}, \\ \text{whence} \quad F(r) &= A_1 H_n^{(1)}(kr) + A_2 H_n^{(2)}(kr) \end{aligned}\right\} \tag{20}$$

where $H_n^{(1)}$ and $H_n^{(2)}$ are Hankel functions, and $k = \omega(gh_2)^{-\frac{1}{2}}$;

$$\left.\begin{aligned} \text{or} \quad h(r) &= h_1(r/r_1)^2, \\ \text{whence} \quad F(r) &= B_1 r^{s_1} + B_2 r^{s_2}, \end{aligned}\right\} \tag{21}$$

where $s_1, s_2 = -1 \pm (1 + n^2 - \omega^2 r_1^2/gh_1)^{\frac{1}{2}}$.

Most of the published work on wave trapping by islands (Longuet-Higgins 1967; Summerfield 1969) is based on two annular regions of constant depth separated by a vertical step. Summerfield invokes a paraboloid (21) to represent a shelving beach, but limits this too by a large vertical step. Figure 11 suggests that a stepped model would hardly do for St Helena, but the form (21) carried down to $h = h_2$ where it is replaced continuously by (20) for all $r \geqslant r_2$, i.e. (17), is more

realistic. Choice of the continuous paraboloid reduces the trapping capabilities of the island, because it does not possess the sharp contrasts in critical wave velocity $(gh)^{\frac{1}{2}}$ necessary for high internal reflexion, or an inner shallow 'shelf' where wave energy can be trapped. Indeed, Longuet-Higgins (1967) pointed out that a power law r^n with $n > 2$ will not trap waves at all. It will be found in fact that the reflecting and resonating properties of the present model are considerably less than in any of the stepped models of similar proportions.

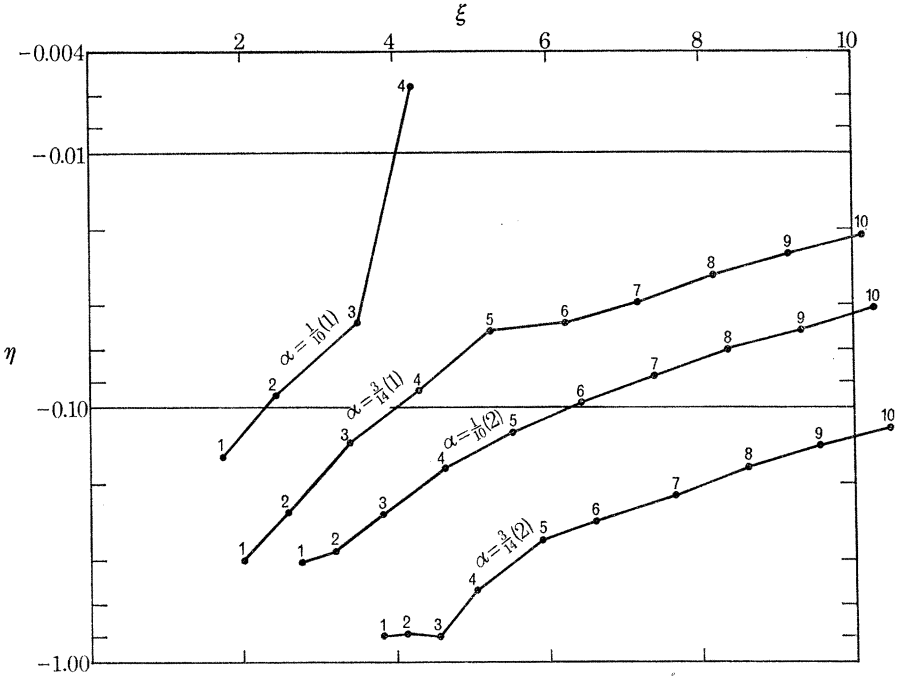

FIGURE 12. The two main sequences of zeros of $G_{n,\alpha}(z)$, $z = \xi + i\eta$, for $\alpha = \frac{3}{14}$, (figure 11, left) and $\alpha = \frac{1}{10}$, and values of n indicated.

The eigenfrequencies are given by the (complex) zeros of a function

$$G_{n,\alpha}(z), \quad (\alpha = r_1/r_2, z = kr_2 = \omega r_2(gh_2)^{-\frac{1}{2}}),$$

determined by setting $A_2 = 0$ to ensure radiation towards infinity, $F'(r_1) = 0$ to ensure transverse currents at the 'coastline', and expressing continuity of F and hF' across $r = r_2$. The result is

$$G_{n,\alpha}(z) = p(1-\alpha^{2q})\, H_n^{(1)}(z) + \{1+q-(1-q)\,\alpha^{2q}\}\, zH_n^{(1)\prime}(z), \tag{22}$$

where $$p = z^2 - n^2,$$

and $$q = (1-p)^{\frac{1}{2}}.$$

As in the cases discussed in depth by Longuet-Higgins (1967), $G_{n,\alpha}(z)$ possesses no *real* eigenfrequencies which would imply perfect trapping with no leakage of energy, but sequences of complex eigenfrequencies $z = \xi + i\eta$ do occur with $\eta < 0$, implying 'leaky' modes with waveforms (18) decaying exponentially in time. Some members of the sequences have $|\eta| \ll 1$, implying a very small but finite decay rate and a condition close to perfect trapping. All the zeros of $G_{n,\alpha}(z)$ within the limits $0 \leqslant \xi \leqslant 10$, $-1 \leqslant \eta < 0$, for the present ratio $\alpha = \frac{3}{14} = 0.2143$ are shown in figure 12. The unit of ξ is equivalent to a frequency $\omega/2\pi = 1.125\,\text{mHz}$ so that the highest frequency at $\xi = 10$ is about a cycle per 90 s. The zeros occur in two sequences labelled (1) and (2), (1) having the lower value of η for each n. The sequences rise on the whole with increasing n, but only very large (and unrealistic) values of n have a damping factor $|\eta| < 0.03$.

This contrasts with the much lower damping obtained by Summerfield (his figures 6.5) for a range of stepped models, showing zeros at for example $n = 7$, $\alpha = 0.2$ with $|\eta| < 10^{-5}$.

Figure 12 also shows the corresponding sequences of zeros for $\alpha = 0.10$. This ratio would apply if, while retaining $r_2 = 28$, we took $r_1 = 2.8$, $h_1 = 0.0392$ km, that is an island of smaller radius but with perhaps a more realistic shoreline depth. Here we see that the damping factor does rise to a smaller negative value at $n = 4$, but for $n \geqslant 5$ the corresponding zeros do not occur, and the second sequence of zeros is insignificant. It might appear from this that resonances to an incoming wave would be confined to $0 < \xi < 4.3$ but this is not so (as will now be shown) since $|G|$ does have a continuing sequence of *minima* along the real frequency axis even where there are no corresponding zeros in the complex plane.

The response of the island model to an incoming plane wave

$$\zeta_\infty = \mathrm{e}^{\mathrm{i}(kx-\omega t)} \equiv \sum_{n=-\infty}^{\infty} \mathrm{i}^n J_n(kr)\, \mathrm{e}^{\mathrm{i}(n\theta-\omega t)} \tag{23}$$

is found by summing the responses to the individual components on the right. For the nth component, we again assume (21) over the paraboloidal shelf, and take

$$F_n(r) = A_1 H_n^{(1)}(kr) + \mathrm{i}^n J_n(kr) \tag{24}$$

for $r > r_2$. The conditions of continuity of F_n and F_n' at $r = r_2$ together with $F_n'(r_1) = 0$ then yield the solution of the nth component of the wave at the shoreline:

$$F_n(r_1) = \mathrm{i}^{n+1} 4q\alpha^{q-1}/\pi G_{n,\alpha}(kr_2), \tag{25}$$

where $q(z)$ is evaluated at $z = kr_2$, and use has been made of the identity

$$J_n(\xi)\, H_n^{(1)\prime}(\xi) - J_n'(\xi)\, H_n^{(1)}(\xi) \equiv 2\mathrm{i}/\pi\xi.$$

Longuet-Higgins and Summerfield show only diagrams of $|F_n(r_1)|$ for individual values of n. They contain very sharp resonance peaks at the frequencies which are close to the real parts of their complex eigenfrequencies, the smaller the damping $|\eta|$, the higher the resonant magnification. Since these peak magnifications commonly exceed 100 in their stepped models, the resonating mode clearly dominates the whole solution. My computations of (25) with $\alpha = \frac{3}{14}$, however, showed resonant magnifications only of order 3 to 4. Furthermore, when the nth mode is first resonating modes lower than n (but not those greater than n) still have magnification of the same order if somewhat lower. Therefore the individual magnifications $|F_n|$ are not typical of the complete solution to the incoming plane wave (23) in the present case.

Figure 13 shows the amplitude of the complete solution

$$\zeta(r_1, \theta, t) = \left(F_0(r_1) + 2\sum_{n=1}^{\infty} F_n(r_1) \cos n\theta\right) \mathrm{e}^{-\mathrm{i}\omega t} \tag{26}$$

for $\theta = 0$ (lee side), 90° (tangential), and 180° (facing the incoming wave). The solutions for $-\theta$ are of course identical with those for θ, because the Earth's rotation is ignored. By the same token, all amplitudes are practically unity for frequencies below about 1 c/h ($\xi < 0.3$) confirming absence of distortion at tidal frequencies. The response is evidently very complicated, and variable with direction. The peak magnifications again do not exceed the background level by very large factors and the occasional dips are too fine to be resolved in a practical experiment. Unlike the stepped models, the peak heights do not greatly increase with frequency. The only common feature of all curves is a steady rise from 1 at zero frequency to about 8 between 2.2 and

PHILOSOPHICAL TRANSACTIONS OF THE ROYAL SOCIETY A MATHEMATICAL, PHYSICAL & ENGINEERING SCIENCES

3.3 mHz ($\xi = 2$ and 3). The broken curve, calculated for $\alpha = 0.1, \theta = 0$, shows a similar character but with higher levels of magnification, as we should expect from the corresponding eigenfrequencies (figure 12).

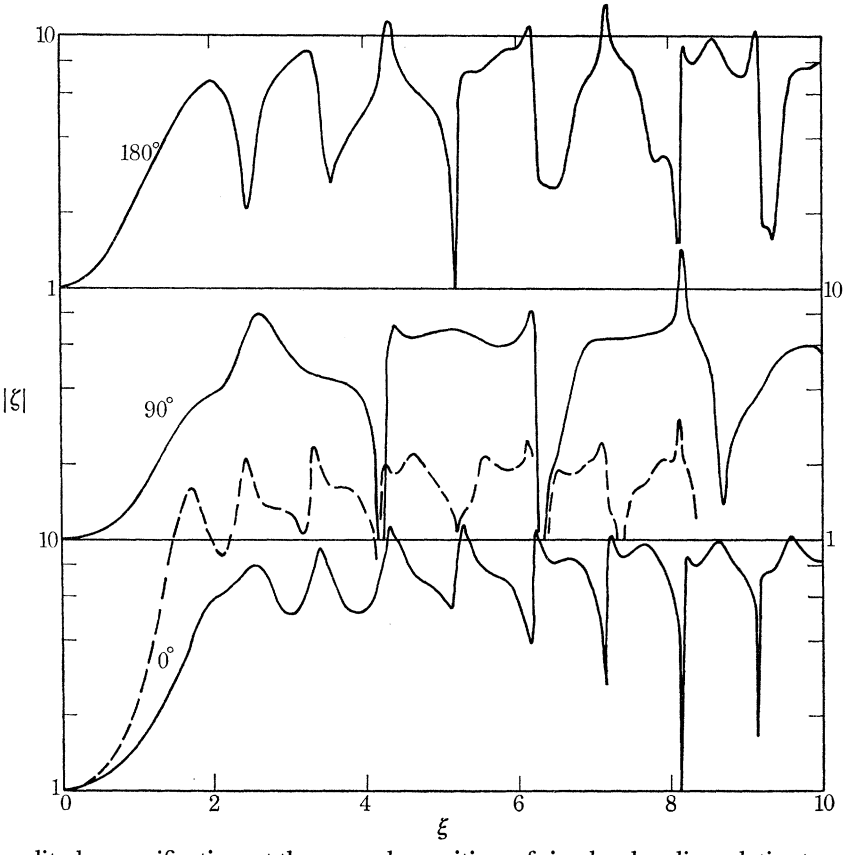

FIGURE 13. Amplitude magnifications at three angular positions of circular shoreline relative to an incoming plane wave, plotted against frequency parameter ξ. Full lines are for $\alpha = \frac{3}{14}$. Broken lines for $\alpha = \frac{1}{10}, \theta = 0$.

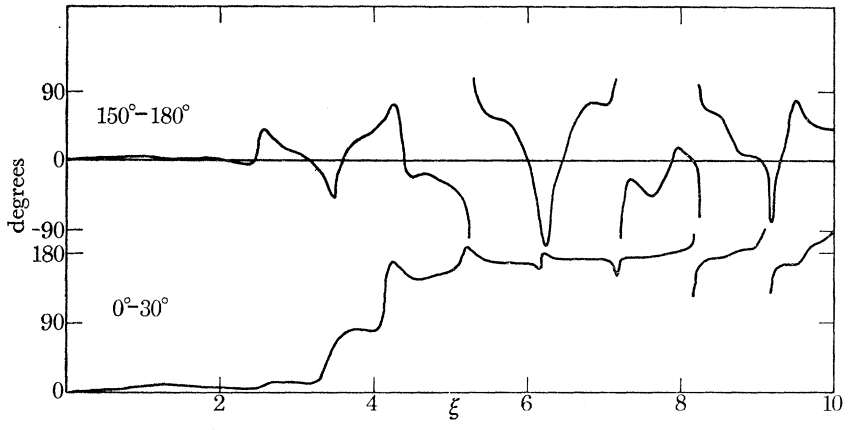

FIGURE 14. Phase lag between positions 30° apart round shoreline for waves as in figure 13.

Figure 14 shows the difference in phase

$$\arg(\zeta(r_1, \theta', t)) - \arg(\zeta(r_1, \theta, t)) \tag{27}$$

for $(\theta', \theta) = (0, 30°)$ and $(150°, 180°)$ respectively, the difference of 30° in polar angle corresponding roughly with the separation of our recorders at Banks Point and James Bay. Here we

see fairly small phase differences of order 10° for frequencies up to 3.3 mHz ($0 \leqslant \zeta \leqslant 3$) where the smaller mode numbers n prevail, then wide variations and dependence on θ at higher frequencies. These variations will cause loss of coherence between recorded signals.

The general effect of geostrophic forces on trapped waves in the frequency range considered was shown by Longuet-Higgins (1967) to be a slight splitting of the resonant frequencies corresponding to the sense of the wave's rotation relative to that of the Earth. We could hardly expect to detect such fine detail in the present poorly tuned system. Longuet-Higgins (1969) also identified another class of (perfectly) trapped waves at frequencies lower than the inertial frequency, which depend entirely on the Earth's rotation. The modal structure is complicated in the general case, but for islands with dimensions of only a few kilometres and typical oceanic depths, there is only one possible member of the class, having a frequency infinitesimally less than the inertial frequency. At the latitude of St Helena the inertial frequency is 0.55 c/d, well outside our medium frequency band and well below the diurnal tides. The energy spectrum of the 39-day tidal record from James Bay and the cross-spectrum of the 24-day records from there and Banks Point (not reproduced here) do not show any significant effect above noise level at 0.55 c/d. Experience elsewhere (for example, see Miyata & Groves 1968) suggests that many years of sea-level records are required to identify such low frequency resonances.

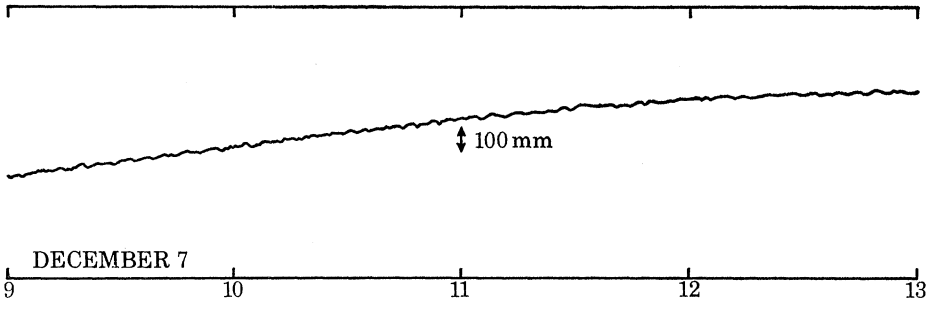

FIGURE 15. Sample of f.m. tide record, 9 to 13 h G.M.T., showing medium waves.

(c) *Analysis of data*

The f.m. tide recorder (appendix A) having a cutoff frequency of about 16 mHZ, medium frequency waves were detectable in its trace almost continually during its 35 days of operation. Amplitudes varied, but the 4 h section reproduced in figure 15 is typical. There we see waves of about 10 mm amplitude and about 12 c/h (3.3 mHz) with others of lower amplitude and higher frequency. The appearance of such waves in the tide record was used as a partial guide to the selection for analysis of pairs of 160 min pneumatic records at fast chart speed from James Bay and Banks Point. Other considerations were strength of trade wind, low swell activity, reliability of timing, etc. The special features of the six pairs selected were as follows:

18 November. Considerable wind and swell; waves in tide record.
19 November. Strongest trade winds of the period (force 8 at Hutts Gate).†
24 November. Very low swell; considerable wind (force 6 at Hutts Gate).†
1 December. No wind; some swell; waves in tide record.
7 December. Little wind; average swell; waves in tide record.
11 December. Average swell; f.m. tide record not working, but waves obvious in pneumatic records.

† The island's meteorological station, 2050 ft above sea level.

Strength of wind may be a means of excitation, in providing a pattern of gusty pressure variations round the island. The significance of swell activity is that some part of the medium-wave record can be due to nonlinear by-products of swell. Apart from the normal hydrodynamic 'wave setup', these include the effects of minor surf among the rocks, 'Bernoulli pressures' caused by wave currents past the considerable obstruction of the underwater units, and also mechanical nonlinearities within the instrument (not designed for high precision measurements). Such motions are likely to be localized, and to distinguish them from genuine trapped waves. I endeavoured to remove them by estimating coherence between each record and its own swell energy.

First, the greater part of the tidal variation was removed from each record in the form of a quartic polynomial fitted optimally over its 160 min span. Then, each tide-free record $\zeta(t)$ was divided into ten precisely timed 1000 s sections† whose Fourier transforms were computed. Now the damping filters of the recorders passed a considerable proportion of the swell motion, which was adequately sampled digitally at 5 s time intervals. I therefore designed real and conjugate highpass swell filters K_p, K'_p, with cutoff frequency about 50 mHz, applied in the following manner:

$$\left.\begin{aligned} S_r(t) &= K_0\zeta(t) + \sum_{p=1}^{12} K_p(\zeta(t+\zeta_p) + \zeta(t-\zeta_p)), \\ S_c(t) &= \sum_{p=1}^{12} K'_p(\zeta(t+\zeta_p) - \zeta(t-\zeta_p)). \end{aligned}\right\} \tag{28}$$

The series $S^2(t) = S_r^2(t) + S_c^2(t)$ is a measure of local mean square swell amplitude, which I correlated with the basic series $\zeta(t)$ at low frequencies by use of Fourier transforms of $S^2(t)$ over the same 1 ks sections.

Coherences between $\zeta(t)$ and $S^2(t)$ were typically about 0.2 to 0.3,‡ and were associated with admittances which had a consistent tendency to negative real parts (the imaginary parts varied between frequencies and from record to record). Thus, the part of $\zeta(t)$ coherent with $S^2(t)$ could be expressed as $-XS^2$, where X was typically about 1 mm/cm² of recorded swell. In terms of real swell this factor should be reduced by about 10^{-1} because the recorded swell was attenuated by the oil filter.

According to the theory of wave setup by radiation stress (Longuet-Higgins & Stewart 1964), the mean sea level is *depressed* by swell waves of local amplitude a in shallow water of depth h by approximately $a^2/4h$. In the present case we have $h = 9m$ giving a depression of 0.003 mm/cm² Pressures due to obstruction of the apparatus to smooth flow would have similar sign and magnitude. Thus, the measured values of X agree in sign with these hydrodynamic effects, but are an order of magnitude greater. The discrepancy is very likely due to mechanical nonlinearities in the recording system.

Having assigned average swell factors X, I then replaced each record $\zeta(t)$ by

$$\zeta'(t) = \zeta(t) + XS^2(t), \tag{29}$$

a series nominally 'corrected' for local nonlinearities, and computed Fourier transforms of $\zeta'(t)$ in the previous 1 ks sections. Figure 16 shows the essential results of correlating these transforms between James Bay and Banks Point. The black circles represent the energy density of $\zeta'(t)$ at Banks, the stepped profile the part which is coherent with $\zeta'(t)$ at James. Their negative separation

† This entailed some minor overlapping, since the total spans were less than 10 ks.
‡ With ensemble average over ten samples, coherences above 0.1 are 'significant'.

on the logarithmic scale is lg (coherence); a separation of 1 corresponds to $\gamma^2 = 0.1$, and closer separation higher coherence. Values for zero frequency, derived from the mean values of 1 ks samples, are not included because they are artifically affected by imperfect removal of the tide, which may also affect the values shown at 1 mHz.

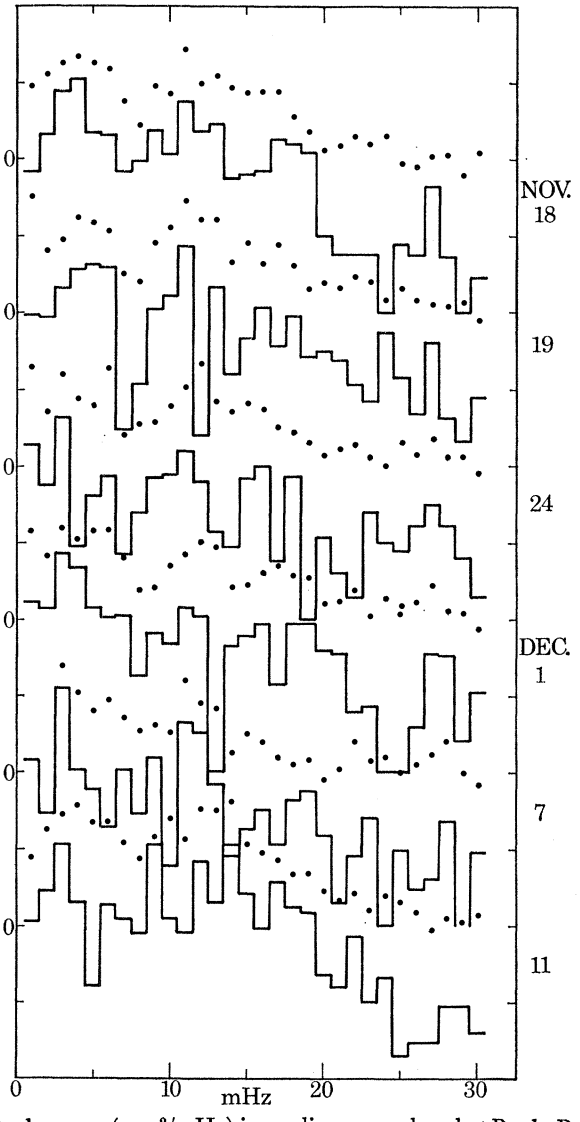

FIGURE 16. Six curves of spectral energy (mm²/mHz) in medium wave band at Banks Point. Circles are total energy; profile is energy coherent with James Bay record. Vertical marks are one (lg) unit apart.

The stepped profiles are the best estimates of trapped wave energy. In general, they tend to rise to a peak around 3–4 mHz, then fall off irregularly at an average rate of about 1 dB/mHz. Energy and coherence at 3 mHz are consistently high in all records. The 3 mHz peak of 7 December stands out particularly well, confirming the reality of the 12/h oscillation evident in figure 15. This record and that of 11 December have the highest total energy levels, suggesting that the strong trade winds of the November records are not the most efficient means of exciting trapped waves, but that some external long wave excitation, possibly emanating from a seismic source in the Pacific Ocean, is more likely to be relevant. The theoretical peaks (figure 13) vary with

direction θ, but assuming an excitation from the southwest one would expect $\theta = 0$ to be not too far out, so that the 3 mHz peaks may well correspond to the lowest mode peaks in the theoretical curves for $\theta = 0$ in figure 13, which predict 2.9 mHz.

At a lower energy level, there seems to be some consistent peaking at 9, 11, 18 and 28 mHz. Of these only 9 mHz has consistently fair coherences, but the rapid changes of amplitude and phase predicted by theory makes coherence improbable at these higher frequencies. The relations between $\zeta'(t)$ at Banks and James at the Fourier transforms of 3 and 9 mHz are detailed in table 7.

TABLE 7. COHERENCES, ADMITTANCES, AND PHASE LEADS (BANKS/JAMES) AT 3 AND 9 mHz

	3 mHz			9 mHz		
	γ^2	$\lvert Z\rvert$	lead	γ^2	$\lvert Z\rvert$	lead
18 Nov	0.45	0.50	−3°	0.29	1.18	+7°
19	0.25	0.78	+12°	0.13	0.53	+28°
24	0.29	0.52	+14°	0.20	0.69	+32°
1 Dec	0.48	0.75	+13°	0.24	0.92	−33°
7	0.49	0.57	−10°	0.36	0.99	−10°
11	0.42	0.71	−5°	0.74	1.62	+6°

The negative phase leads on the days of highest medium-wave activity supports the hypothesis of wave trapping excited by an incoming wave from the southwest. The strong SE trade winds on 19 and 24 November may well have been feeding medium wave energy round Buttermilk Point towards the southwest, accounting for the positive phase leads at Banks on those days. Phase magnitudes are in keeping with the low frequency theoretical values in figure 14. It is not clear why the amplitude at Banks should be consistently lower than at James, but details of coastal topography may be responsible. The results at 9 mHz are consistent with roughly equal amplitudes and rather greater phase differences, as one would expect from the higher trapped modes presumably involved.

Certain features of the results then are in accordance with the idealized wave-trapping theory, although one would need much longer records and samples from other points round the island to resolve any finer details. The major discrepancy is the steady fall in energy towards higher frequencies. Assuming the spectrum of incident waves is more or less uniform over this band this is almost certainly due to scattering at topographical irregularities such as Speery Ledge which should become increasingly effective at the higher mode numbers. Such 'roughness' scattering must ultimately supersede the radiation conditions imposed by the smooth boundary theory for higher n, whose resonance peaks are in any case much less than in wall-sided models with shallow shelves.

The author and his colleagues are grateful to the Hydrographer of the Navy, and to Commander J. Paton and his officers in H.M.S. *Vidal* for transport and assistance in many other respects; to the (then) Acting Governor of St Helena, Mr I. C. Rose, for providing facilities at Jamestown Wharf, and to Mr W. G. Tatham for information on the sites of historical observatories. Messrs Solomon's team of boatmen gave valuable assistance, especially at the Banks Point installation. The United States Coast and Geodetic Survey provided tidal records from Ascension and Tristan da Cunha, and the Brazilian Ministerio da Marinha provided records from Trindade. Roderick N. B. Smith assisted with several of the computations and diagrams.

PHILOSOPHICAL TRANSACTIONS OF THE ROYAL SOCIETY A MATHEMATICAL, PHYSICAL & ENGINEERING SCIENCES

Appendix A. The frequency-modulated pressure recorder for waves and tides

By J. S. Driver

General

The N.I.O. f.m. pressure recorder was originally made in a valve version in 1963 and was transistorized in 1968 to create a more compact unit of lower power consumption allowing operation from 'car type' 12 V batteries as well as from mains. Both these versions were designed primarily to measure sea waves with frequencies between 0.04 and 0.5 Hz. For the St Helena expedition the transistorized instrument was modified to record lower frequency waves and tides. A block diagram of the modified instrument is shown in figure 17.

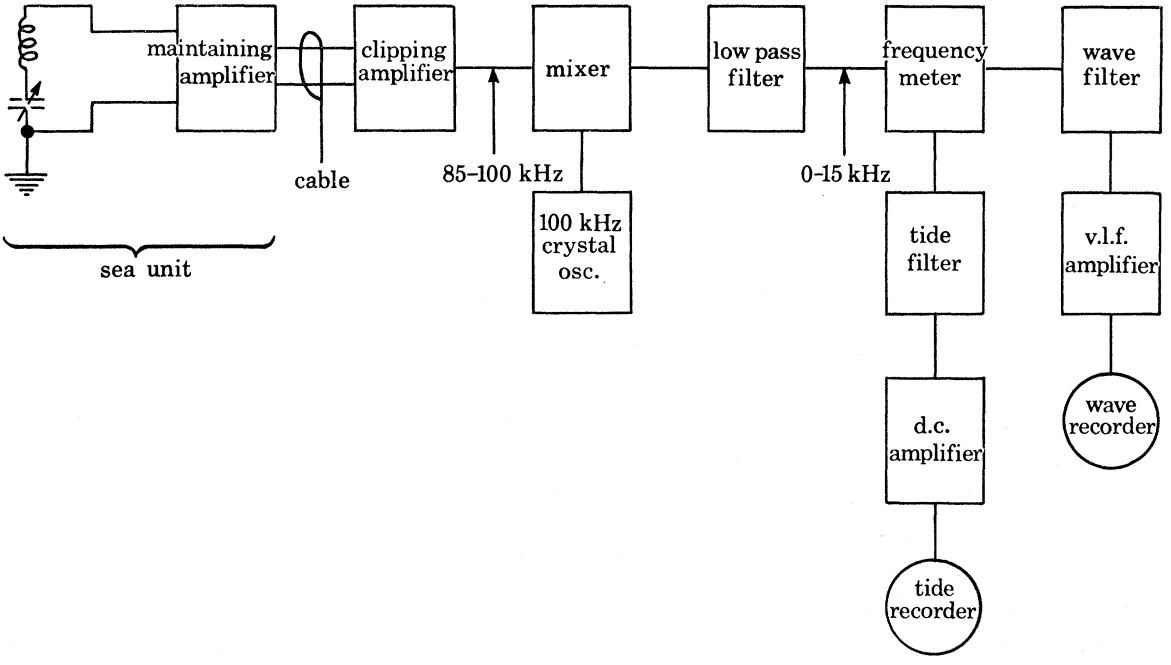

Figure 17. Block diagram for f.m. tide and wave recorder.

Sea unit

The transducer is an absolute pressure gauge and measures fluctuating pressures on the sea bed in shallow water. It has been described in some detail by Harris & Tucker (1963). The wave and tide data are transmitted along a cable back to the shore by means of a frequency modulated system. A technique whereby both signal and supply current are passed along the same conductor enables a two-core armoured cable to be used; the transducer requires only a 6 V supply.

Shore unit

The nominal 95 kHz frequency modulated signal is passed first to a clipping amplifier, the input of which will accept 20 dB attenuation of the sea unit signal before the output is affected, this corresponding to about 3 km of a typical armoured cable. The 95 kHz is then mixed with the output from a 100 kHz crystal oscillator and the frequency difference is selected by the low pass filter and used to drive a Schmitt trigger. The existence of a 'plug in' crystal oscillator in the

shore unit allows convenient compensation for varying depths of installation without dismantling the sea unit, i.e. a difference frequency within the range 0 to 15 kHz can be maintained at all times. The Schmitt trigger provides the frequency meter or discriminator circuit with a constant amplitude f.m. signal; the meter output is then a voltage directly proportional to applied pressure and hence tide + wave elevation. At this point it was possible to insert filters to separate waves and tides before finally amplifying the signals to drive the recorder galvanometers. These very low frequency/d.c. amplifiers contain matched pairs of transistors to reduce temperature effects.

The wave filter has its low frequency cut off at 1/60 Hz (a time constant of 60 s) whilst the high-frequency attenuation becomes significant at frequencies higher than 0.5 Hz. The tide filter time constant is arranged to coincide with that of the wave filter at 60 s; thus its pass band extends from 1/60 Hz to 0.

Chart recorder displays were used for both sets of information. The tide recorder was wired to run continuously at the rate of 60 mm/h, hence consuming one 20 m chart every 2 weeks while the wave data were sampled by recording for 2 h 40 min once every 12 h using a chart speed of 120 mm/min. An internal battery driven clock was programmed to switch the wave chart drive on, so that mains supply interruptions would not affect the wave sampling interval. In order to maintain good timekeeping throughout the period of installation a quartz crystal controlled clock was fitted to the unit, also driven from its own battery supply.

Installation history

A length of 150 m of stainless steel wire armoured cable was used to connect the transducer to the shore unit. The sensitivity of the system was 658 Hz/m as calculated before hand from tests in a pressure vessel. There were two main operational problems: (1) a mean frequency drift equivalent to about 200 mm/month originating from the transducer. This drift is characteristic of these pressure transducers but could be removed by comparison with the stillwell readings. (2) The available mains supply was subject to electrical interference and suffered some considerable volt drop under high load conditions. The mains-borne interference caused the occasional 'spike' or short-term disturbance on the tide record but these could be smoothed out by eye. The mains regulation problem was largely overcome by good power supply stabilization circuits.

The transducer finally stopped working 3 days before the end of our stay due to an underwater leak in the cable termination chamber.

Appendix B. Analysis of tidal extrema

If we assume the sea level $\zeta(t)$ consists of a pure tide of the form specified plus a noise error $e(t)$ uncorrelated with it, then the minimum mean values of the left and right squared brackets in equation (3) are respectively

$$\sigma_0^2 = \langle e^2(t) \rangle \quad \text{and} \quad \sigma_1^2 = \langle \dot{e}^2(t) \rangle.$$

According to the normal least-squares formalism, we then have for the time constant in (3)

$$K = \sigma_0/\sigma_1 = (24/2\pi) \left[\int_0^\infty E(f)\, \mathrm{d}f \Big/ \int_0^\infty f^2 E(f)\, \mathrm{d}f \right]^{\frac{1}{2}}, \tag{B 1}$$

where $E(f)$ is the energy (variance) density spectrum of $e(t)$ with f in cycles per day.

For Ascension Island, $E(f)$ was computed from the 29 d hourly series, 1 February to 1 March 1959 after subtracting a conventional tidal synthesis from $\zeta(t)$. On summing spectral increments, the estimates for the two integrals in B 1 were respectively 999 and 3929 $\mathrm{mm^2\,d^{-2}}$, giving $K = 1.93$ h. This value was used in the subsequent analysis.

Assume for simplicity of illustration that only one element $c_1(t) = a_1(t) + ib_1(t)$ of the tidal potential is being fitted to the data, so that (3) becomes

$$V = \sum_n [\{u_0 + u_1 a_1(t_n) + v_1 b_1(t_n) - \zeta(t_n)\}^2 + K^2\{u_1 \dot{a}_1(t_n) + v_1 \dot{b}_1(t_n)\}^2].$$

The normal equations for minimum V are

$$\left.\begin{aligned} u_0 + \quad & \overline{a_1} u_1 + \quad & \overline{b_1} v_1 &= \overline{\zeta}, \\ \overline{a_1} u_0 + \quad & (\overline{a_1^2} + K^2\overline{\dot{a}_1^2})\, u_1 + & (\overline{a_1 b_1} + K^2\overline{\dot{a}_1 \dot{b}_1})\, v_1 &= \overline{\zeta a_1}, \\ \overline{b_1} u_0 + & (\overline{a_1 b_1} + K^2\overline{\dot{a}_1 \dot{b}_1})\, u_1 + & (\overline{b_1^2} + K^2\overline{\dot{a}_1^2})\, v_1 &= \overline{\zeta b_1}, \end{aligned}\right\} \tag{B 2}$$

where a bar denotes the operation $N^{-1}\sum_n$, where $N = \sum_n 1$. The equations for the standard application of the 'response' method are similar to (B 2) with $K = 0$ and the summation taken over equally spaced times.

It is convenient to eliminate the arbitrary constant term u_0, so that the equations for the principal weights u_1 and v_1 become

$$\left.\begin{aligned} (\sigma(a_1, a_1) + K^2\overline{\dot{a}_1^2})\, u_1 + (\sigma(a_1, b_1) + K^2\overline{\dot{a}_1 \dot{b}_1})\, v_1 &= \sigma(\zeta, a_1), \\ (\sigma(a_1, b_1) + K^2\overline{\dot{a}_1 \dot{b}_1})\, u_1 + (\sigma(b_1, b_1) + K^2\overline{\dot{b}_1^2})\, v_1 &= \sigma(\zeta, b_1), \end{aligned}\right\} \tag{B 3}$$

where

$$\sigma(x, y) = \overline{yx} - \bar{x}.\bar{y}.$$

Thence

$$V_{\min} = \sigma(\zeta, \zeta) - u_1\sigma(\zeta, a_1) - v_1\sigma(\zeta, b_1). \tag{B 4}$$

One may not, however, ignore u_0 altogether, because $\overline{a_1}$ and $\overline{b_1}$ are not necessarily very small when evaluated over the selective times of extrema t_n, especially if nonlinear terms are present. The extension of B 3 and B 4 to a more general set of tidal potentials $a_s(t-\tau) + ib_s(t-\tau)$ is straightforward.

It remains to explain how the potentials and their time derivatives are evaluated at arbitrary times t_n from computed series $c_s(t)$ with t at precise G.M.T. hours. An adumbration of the method was given in another context in pp. 199–200 of Cartwright (1969), but it can be stated more succinctly as follows:

Since any tidal function $c_n^m(t)$ of species m consists essentially of a slowly modulated carrier wave of frequency $m\omega$ radians/hour,† we may write

$$c_n^m(t) = C(t)\, \mathrm{e}^{-\mathrm{i}m\omega t}, \tag{B 5}$$

where $C(t)$ is a low-frequency complex variable of at most a few cycles per month. For any four consecutive hours, say $t = -1, 0, 1, 2h$, $C(t)$ may be accurately represented by a cubic expression

$$C(t) \doteqdot C(0) + \gamma_1 t + \gamma_2 t^2 + \gamma_3 t^3, \tag{B 6}$$

with the coefficients γ_n evaluated from its four values computed from (B 5). Within the interval $0 \leqslant t \leqslant 1$ (B 5) and (B 6) are then used to define $c_n^m(t)$ and its derivative

$$\dot{c}_n^m(t) = -\mathrm{i}m\omega c_n^m(t) + \dot{C}(t)\, \mathrm{e}^{-\mathrm{i}m\omega t}.$$

† Any value of ω reasonably close to 2π radians/lunar day will do. $\omega = 0.254$ rad/h is a convenient choice. Solar variations are absorbed in the modulation.

PHILOSOPHICAL TRANSACTIONS OF THE ROYAL SOCIETY A MATHEMATICAL, PHYSICAL & ENGINEERING SCIENCES

Appendix C. Tidal constants for Simons Bay and Ascension Island

(a) *Response weights for Simons Bay*

The data, hourly sea levels from 1 January 1959 to 23 December 1967 were analysed by the ordinary 'response method' (Munk & Cartwright 1966; Cartwright 1968). Nonlinear variables were included, but were found to give negligible prediction variance, so are omitted from this list. Time lags are in 2 d units.

		weights				weights	
variable	lag	real	imag.	variable	lag	real	imag.
χ_1^0	0	−6.356700	2.753919 ($\chi_1^{0\prime}$)	c_3^1	1	0.798218	−0.075489
c_2^0	1	−0.039218	—		0	−1.697978	0.978294
	0	0.033690	—		−1	0.688445	−0.050924
c_3^0†	1	2.095468	—	χ_2^2	0	−5.292905	−3.846307
	0	1.078771	—	c_2^2	2	0.088519	0.323625
χ_1^1	0	−0.329798	−0.008640		1	0.169307	−0.714411
χ_2^1	0	−0.660782	−1.310794		0	0.391528	−0.153250
c_2^1	2	−0.028643	0.061901		−1	−0.072194	−0.068887
	1	−0.163154	0.067738		−2	−0.010672	0.067168
	0	0.338765	0.069503	c_3^2	1	−0.815962	−0.958777
	−1	−0.097268	−0.092247		0	−0.547665	1.281154
	−2	0.006014	0.044160		−1	0.688744	−0.587374

† For significance of c_3^0 at Simons Bay, see text, § 3 (*b*).

(b) *Response weights for Ascension Island*

The data, consisting of all extrema between 21.5 June 1958 and 21.5 June 1959, were analysed by the method outlined in appendix B. Nonlinear terms were negligible. The notation is as in (*a*) above.

		weights				weights	
variable	lag	real	imag.	variable	lag	real	imag.
χ_1^0	0	8.919976	1.409670 ($\chi_1^{0\prime}$)	c_3^1	0	−0.396329	−0.344636
c_2^0	1	0.098529	—	χ_2^2	0	1.541226	−1.582641
	0	−0.112051	—	c_2^2	1	0.030025	0.225652
χ_1^1	0	0.085366	0.093279		0	−0.545023	−0.239080
c_2^1	1	−0.055455	−0.312263		−1	0.086618	0.157854
	0	−0.099154	0.293112	c_3^2	0	−0.439371	0.324388
	−1	0.052622	−0.061071				

(c) *Harmonic constants for Ascension Island*

These were derived from the above weights after conversion to admittances (drawn in figure 3) and multiplying by the harmonic constants of the gravitational and radiational potentials (Cartwright & Tayler 1971). H and G ($= g$) are in the conventional notation.

symbol	type	H/mm	$G°$	symbol	type	H/mm	$G°$
Sa	rad	36.3	98.98†	$2N_2$	grav	11.7	149.70
Q_1	grav	8.9	144.57	N_2	grav	73.9	161.53
O_1	grav	25.5	196.02	M_2	grav	328.4	176.82
M_1	grav	1.9	268.73	L_2	grav	8.4	151.46
P_1‡	grav	15.3	318.11	S_2	grav	132.8	198.63
S_1	rad	1.8	132.68		rad	12.3	045.76
K_1‡	grav	49.6	325.41		total	121.9	196.00
J_1	grav	4.6	364.08	K_2	grav	35.9	199.17
					rad	1.1	045.76
					total	34.9	198.38

† The annual component of χ_1^0, refers to the northern summer solstice whereas $G(Sa)$ conventionally refers to the vernal equinox. ‡ The radiational potential χ_1^1 has negligible contribution to P_1 and K_1. χ_2^1 was ignored.

PHILOSOPHICAL TRANSACTIONS OF THE ROYAL SOCIETY A MATHEMATICAL, PHYSICAL & ENGINEERING SCIENCES

References

Barber, N. F. & Ursell, F. 1948 The generation and propagation of ocean waves and swell. *Phil. Trans. R. Soc. Lond.* A **240**, 527–560.

Bogdanov, K. T. & Magarik, V. A. 1967 Numerical solutions to the problem of distribution of semidiurnal tides M_2 and S_2 in the World Ocean. *Dokl. Akad. Nauk SSSR* **172**, no. 6, 1315–1317.

Cartwright, D. E. 1968 A unified analysis of tides and surges round north and east Britain. *Phil. Trans. R. Soc. Lond.* A **263**, 1–55.

Cartwright, D. E. 1969 *Proc. I.H.B. Symposium on Tides, held Monaco, April* 1967, pp. 195–200. Unesco publ.

Cartwright, D. E., Munk, W. H. & Zetler, B. D. 1969 Pelagic tidal measurements. *EOS, Trans. Am. geophs. Un.* **50**, no. 7, 472–477.

Cartwright, D. E. & Tayler, R. J. 1971 New computations of the tide-generating potential. *Geophys. J. R. astr. Soc.* **23**, no. 1, 45–73.

Collar, P. G. & Spencer, R. 1970 A digitally recording offshore tide gauge. *Proc. I.E.R.E. Conf. Electronics in Ocean Tech.* pp. 341–352.

Defant, A. 1961 *Physical oceanography*, vol. 2. London: Pergamon Press.

Dietrich, G. 1944 Die Schwingungssysteme der halb- und eintägigen Tiden in den Ozeanen. *Veröff. Inst. Meeresk. (Berlin)*, no. 41.

Eyriès, M. 1968 Marégraphes de grandes profondeurs. *Cah. océanogr.* **20**, 355–367.

Filloux, J. H. 1971 Deep sea tide observations from the northeastern Pacific. *Deep Sea Res.* **18**, 275–284.

Garrett, C. J. & Munk, W. H. 1971 The age of the tide and the Q of the oceans. *Deep Sea Res.* **18**, no. 5, 493–503.

Grace, S. F. 1930 The semi-diurnal lunar motion of the Red Sea. *Mon. Not. R. Astr. Soc. geophys. Supp.* **2**, no. 6, 273–296.

Greenwood, J. A., Nathan, A., Neumann, G., Pierson, W. J., Jackson, F. C. & Pease, T. E. 1969 Radar altimetry from a spacecraft. *Remote Sensing of Environment* **1**, 59–80.

Hansen, W. 1952 Gezeiten des Meeres. In Landolt-Börnstein. *Zahlenwerte und Funktionen* **3**, 516. Berlin: Springer.

Hansen, W. 1966 Preliminary scheme of deep sea tidal measurements based on tidal theory. *Mitt. Inst. Meeresk. Univ. Hamburg.* no. 6.

Harris, M. J. & Tucker, M. J. 1963 A pressure recorder for measuring sea waves. *Instrum. Pract.* **17**, 10, 1055–1059.

Hendershott, M. 1970 Cotidal map for M_2 reproduced in: Hendershott, M. & Munk, W. H. 1970 'Tides'. *Ann. Rev. Fl. Mech.* **2**, 205–224.

Lalande, J. de 1781 *Astronomie*, tome 4. Paris.

Lamb, H. H. 1964 The role of atmosphere and oceans in relation to climatic changes and the growth of ice sheets on land. In *Problems in palaeoclimatology* (ed. A. E. M. Nairn), pp. 332–347. London: Interscience.

Longuet-Higgins, M. S. 1967 On the trapping of wave energy round islands. *J. Fluid Mech.* **29**, no. 4, 781–821.

Longuet-Higgins, M. S. 1968 Double Kelvin waves with continuous depth profiles. *J. Fluid Mech.* **34**, no. 1, 49–80.

Longuet-Higgins, M. S. 1969 On the trapping of long-period waves round islands. *J. Fluid Mech.* **37**, no. 4, 773–784.

Longuet-Higgins, M. S. & Stewart, R. W. 1964 Radiation stresses in water waves. *Deep Sea Res.* **11**, 529–562.

Maskelyne, N. 1762*a* Observations on a clock of Mr J. Shelton, made at St Helena. *Phil. Trans. R. Soc. Lond.* **52**, 434.

Maskelyne, N. 1762*b* Observations on the tides in the island of St Helena. *Phil. Trans. R. Soc. Lond.* **52**, 586–606.

Mason, C. 1762 Observations for proving the going of Mr Ellicott's clock at St Helena. *Phil. Trans. R. Soc. Lond.* **52**, 534.

Meeus, J. 1962 Tables of Moon and Sun. Kesselberg Sterrenwacht, Kessel-Lo, Belgium.

Miyata M. & Groves, G. W. 1968 Note on sea level observations at two nearby stations. *J. geophys. Res.* **73**, 12, 3965–3967.

Munk, W. H. 1962 Long ocean waves. In *The sea* (ed. M. N. Hill), pp. 647–663. London: Interscience.

Munk, W. H. 1968 Once again—tidal friction. *Q. Jl R. Astr. Soc.* **9**, no. 4, 352–375.

Munk, W. H. & Cartwright, D. E. 1966 Tidal spectroscopy and prediction. *Phil. Trans. R. Soc. Lond.* A **259**, 533–581.

Munk, W. H., Miller, G. R., Snodgrass, F. E. & Barber, N. F. 1963 Directional recording of swell from distant storms. *Phil. Trans. R. Soc. Lond.* A **255**, 505–584.

Munk, W. H., Snodgrass, F. E. & Wimbush, M. 1970 Tides offshore: transition from California coastal to deep-sea waters. *Geophys. Fluid Dyn.* **1**, 161–235.

Pekeris, C. L. & Accad, Y. 1969 Solution of Laplace's equations for the M_2 tide in the world oceans. *Phil. Trans. R. Soc. Lond.* A **265**, 413–436.

Proudman, J. 1928 The determination of earth-tides by means of water-tides in narrow seas. *Bull. Sect. Ocean. Cons. Int. Recherches.* **11**, 1–6.

PHILOSOPHICAL TRANSACTIONS OF THE ROYAL SOCIETY A MATHEMATICAL, PHYSICAL & ENGINEERING SCIENCES

Rhines, P. R. 1969 Slow oscillations in an ocean of varying depth (*I*). *J. Fluid Mech.* **37**, 161–189.
Snodgrass, F. E. 1968 Deep sea instrument capsule. *Science*, **162**, 78–87.
Snodgrass, F. E., Groves, G. W., Hasselmann, K. F., Miller, G. R., Munk, W. H. & Powers, W. H. 1966 Propagation of ocean swell across the Pacific. *Phil. Trans. R. Soc. Lond.* A **259**, 431–497.
Summerfield, W. C. 1969 On the trapping of wave energy by bottom topography. *Res. Pap. H. Lamb Centre Oceanogra. Res., Flinders U. South Australia*, no. 30.
Tiron, K. D., Sergeev, Yu. N. & Michurin, A. N. 1967 Tidal charts for the Pacific, Atlantic and Indian Oceans. *Vest. Leningrad. Univ.—Geol. and Geog.* ser. no. 24, 123–135.
Wunsch, C. 1967 The long-period tides. *Rev. Geoph.* **5**, no. 4, 447–475.

PHILOSOPHICAL TRANSACTIONS OF THE ROYAL SOCIETY A MATHEMATICAL, PHYSICAL & ENGINEERING SCIENCES

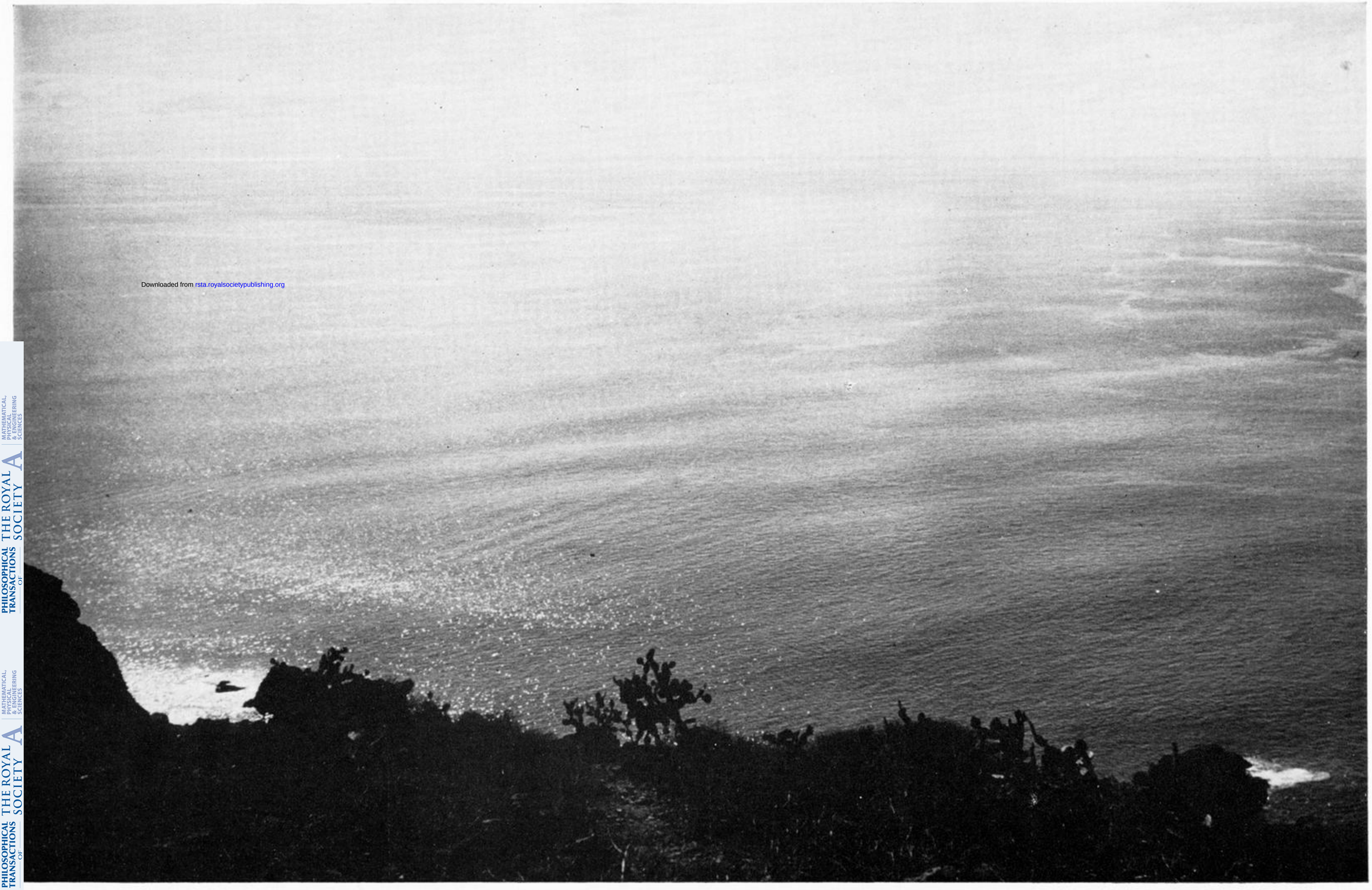

FIGURE 18. View of swell off Thompsons Bay approaching from the southwest (left of picture) on 9 November about 16 h. The shorter waves in part of the foreground are due to scattering by an offshore islet.